FRACTURE STUDIES ON OPTICAL FIBRES

Thesis submitted for the C.N.A.A.
degree of Master of Philosophy

by

LEE ENG WAH

This work was conducted at Middlesex
Polytechnic in collaboration with
Standard Telecommunication Laboratories.

June 1983

CONTENTS

LIST OF FIGURES

LIST OF TABLES

ABSTRACT

FRACTURE STUDIES ON OPTICAL FIBRES
Lee Eng Wah

The fracture behaviour of optical fibre was studied both in pure tension and combined tension and torsion. The results were analysed in terms of failure statistics and fracture mechanics. Electron microscopy techniques were employed to ascertain possible flaw size and their location which may contribute to the failure of the fibre. Three flaw mechanisms were shown to exist arising from large surface flaws, bulk flaws and inherent surface defects due to the pulling process.

The long term mechanical reliability of optical fibre is of major concern to the manufacturers. The phenomenon of subcritical crack growth was investigated by dynamic fatigue tests both in air as well as in acidic and alkaline environments. The parameter 'stress corrosion susceptibilities' in the various environments were evaluated. Results indicated that the presence of water in the environment significantly contributes to the subcritical crack growth rate in the fibre. In solutions, the presence of OH^- ions further enhances this effect. Removal of water and OH^- ions after presoaking the fibre was shown to effect a complete recovery of the strength.

Design diagrams for optical fibre were constructed. These diagrams incorporate the statistical nature of the strength as well as the time dependent behaviour of the fibre. The value of such a diagram is to estimate the proof stress required for a given working stress and a given length of time if no failure is to be assured.

ACKNOWLEDGEMENTS

I wish to thank the Middlesex Polytechnic and Standard Telecommunication Laboratories Limited for providing facilities, materials and financial support. In particular, I would also like to thank Dr C J Spears and Mr M M Ramsay for their help as supervisors to my work and Mrs V Norman for typing the manuscript so efficiently. My grateful thanks are due to Mr G Adie and Mr M Hart for their technical support and Dr J Lees and Mr I Scanlon for their valuable discussions.

CHAPTER 1

1.1 INTRODUCTION

Beacon fires were used to break the news of the fall of Troy and the King's homecoming to his Queen, Clytemaestra in 1084 B.C. at the palace of Argos in Greece. Until quite recent times the call for rapid communications has always invariably been due to military demands rather than to social or commercial needs, and the situation in France was no exception. The appearance of the system of semaphore telegraphs, designed by Claude Chappe, turned the military balance towards revolutionary France. The Chappe system of telegraphs rendered invaluable service to the French government for more than half a century and when it was finally closed down in 1852, it comprised a total of 556 stations with a total length of more than 4000 kilometres.

By the middle of the nineteenth century, light communication techniques had been mainly superceded; firstly by the electric telegraph and, later, with the advent of telephone and radio communication.

Interest in optical communication was revived as a result of the achievement of the first laser[1] in the early sixties. The coherent nature of laser light enabled optical frequencies to be viewed as an extension of the radio and microwave spectrum.

Transmitting optical signals in the form of laser light through the atmosphere was generally too unreliable due to interference of fog, rain and dust. Despite these problems, optical communication systems transmitted through the atmosphere were developed for distances of a few hundred metres. Such modest links have been built for linkage of outside television camera to its base vehicle.

Laser light, guided through a gas filled pipe with lenses placed at regular intervals of about one hundred metres to collimate the beam, was investigated as a possible transmission medium[2]. Telecommunication systems, based on this technique, offered remarkable performance in terms of bandwidth and repeater separations. Owing to the complexity and high cost to build and install, this system did not meet any real need.

Optical fibre, with core and cladding structure, invented in 1954[3,4], described its use as a medium for transporting optical images such as fibrescope. It was not until 1966, after careful studies that Kao and Hockham[5] proposed its use in a cable as a long distance transmission medium in optical communication. Their idealised system is as shown

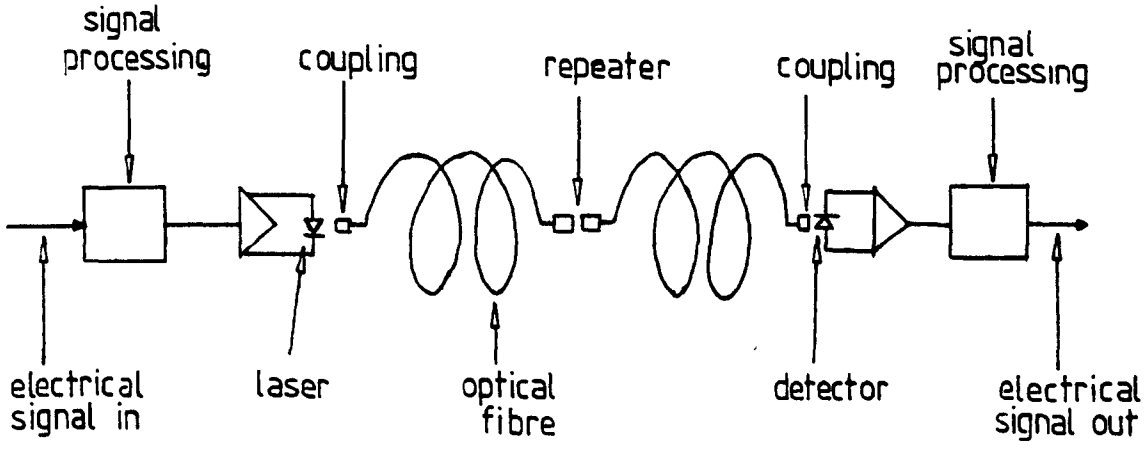

Components of Optical Fibre Communication System

The optical source to be used was a Gallium Arsenide laser, optical fibre was to carry the signals and the detector was anticipated to be a silicon photodiode. This became the basis for the development of optical fibre communication system.

Rapid technological advances followed in optical components such as sources, detectors, lenses and fibres. There was increasing evidence that optical fibre communication would become the next generation of telecommunication system.

Optical fibre advantages become obvious with the very low losses incurred, typically: 2.5 db/km at 850 nm, 0.7 db/km at 1300 nm, and 0.3 db/km at 1550 nm. High bandwidth, coupled with relatively small fibre, require fewer repeaters, and so enable a more efficient utilisation of duct space. As such, buried electronics (e.g. repeaters) in the cities, could be eliminated and confined to terminal buildings, thus making installation, operation and maintenance of the system much easier and cheaper. This is particularly attractive to civil telecommunication usages.

The components of the optical fibre system are virtually metal-free and, therefore, electromagnetic interference can be eliminated. Cables may be made metal-free or not dependent on the application. Such a feature has great benefit to military users where sensitive electronic systems are often packaged alongside electrical power system in aircraft, ships and vehicles.

The fused silica raw material for the manufacture of optical fibre is relatively cheap and abundant. This has another major advantage over conventional systems, as copper is getting scarce and their supplies often unreliable.

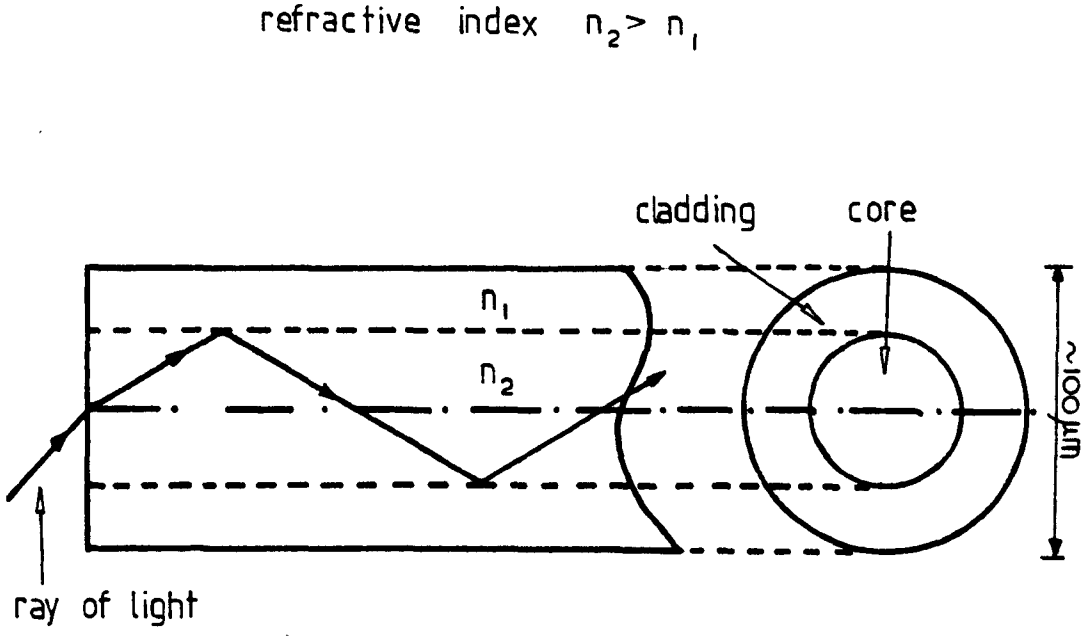

LIGHT PROPAGATION THROUGH OPTICAL FIBRE

Current optical fibre itself is a thin fused silica fibre of the order of 100 μm having a core/cladding structure. The core is carefully doped to produce a higher refractive index. Total internal reflection occurs when light enters the core material of higher refractive index and strikes the interface of the lower refractive index cladding. The interface reflects the light through the fibre until it is emitted at the end.

Initial work in fabricating optical fibres for communication was mainly concerned with reducing its optical losses due to absorption, scattering and microbending. This was necessary in order to allow sufficiently long spacings so as to be competitive with existing communication systems. It is now possible to produce extremely low loss fibre by the modified chemical vapour deposition technique[6]. This process consists of depositing layers of doped high

silica glasses inside a silica support tube which is subsequently collapsed to form a solid rod preform. The preform is passed into a high temperature furnace and drawn into fibres.

As extremely low loss optical fibre has been achieved, its mechanical properties become a major concern. Kilometre lengths of fibre without fracture-producing flaws are necessary. The fibres to be incorporated into a cable will have to withstand the mechanical stresses imposed upon them during manufacture, installation and service life.

Early attempts to produce long lengths of fibre suffered severe setbacks because the mechanical strength could not be controlled. The highly reactive surface of the fibre on exposure to atmosphere caused flaws to nucleate, so providing potential fracture sites. Also, as the fibre came into direct contact with the take-up drum, more flaws were generated. These surface problems were largely overcome by on-line coating with a silicone resin (primary coating) as soon as the fibre was pulled. This primary coating served as a barrier against the environmental interaction and also protected the fibre from minor impact and abrasion during other subsequent processings.

Consequently, the pristine strength which was believed to exist as soon as the fibre was pulled was maintained and relatively long lengths of flaw free fibre could be achieved. Although the primary coating inhibited to a great degree the nucleation of large surface flaws, it was found that they could not be totally eliminated. It was, therefore, very important to identify the particularly large flaws which contributed to the low strength so that steps could be taken to eliminate or reduce their occurrance.

Studies have shown that a mechanical strength of fused silica fibre is time dependent. This is recognised[7] to be due to subcritical crack growth under conditions of

stress and potentially corrosive environment. The underlying mechanism to this phenomenon, often termed static fatigue is not fully understood. It is, therefore, important that careful study and evaluation be carried out in order to predict its long term strength.

The aim of the present project is to identify the various types of flaws, their sources of origin and their distribution. Both tensile and combined tension and torsion test methods for the application to optical fibre have been developed to study the effect of the fibre under combined stress systems. Optical fibres were also tested at different strain rates and under different environments to investigate the sub critical crack growth.

The results obtained have been treated in terms of failure statistics and fracture mechanics. Scanning electron microscope has been used to examine the fracture surfaces and possible models of flaw and fracture mechanisms have been identified.

1.2 INTRODUCTION TO MATERIALS

The optical fibre used is made up of a silica based glass core which is normally doped with boric oxide (B_2O_3), germanium oxide (GeO_2), and phosphorus pentoxide (P_2O_5). The cladding is usually of silica dope with boric oxide. Boric oxide lowers the refractive index and is, therefore, included in the cladding. The GeO_2 and P_2O_5 dopants in the core are necessary to achieve higher refractive index as well as to improve deposition rate. Also, they provided a more compatible viscosity thus enabling a better dimensional stability. Step-index fibre has a core of uniform glass composition, whereas the graded-index fibre has a compositional change through the diameter of the core to obtain a near parabolic index profile,as shown below :

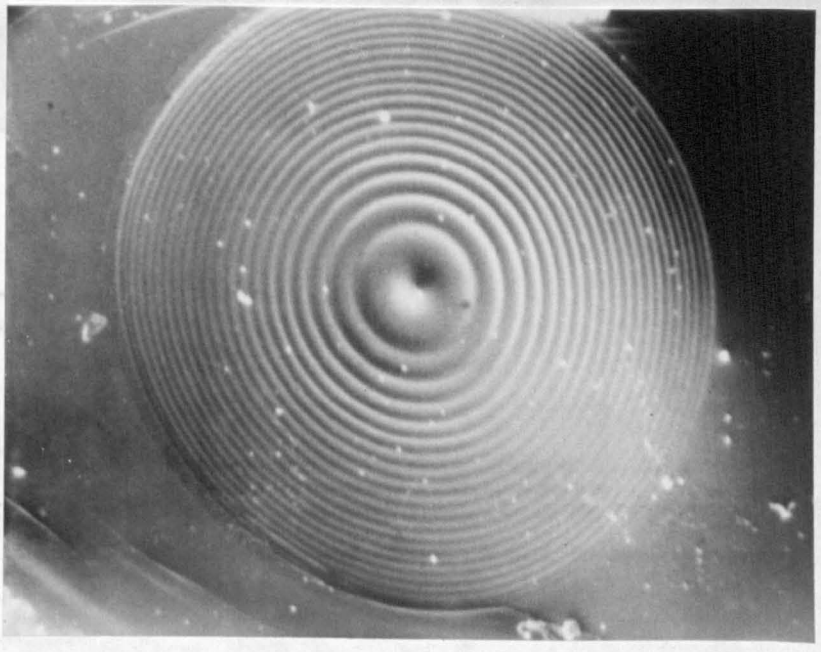

SEM Micrograph of the core of a graded index fibre showing the deposited layers of dopants to achieve a near parabolic index profile.

A thin layer of silicone resin was applied to the fibre prior to coating with polypropylene. The overall structure of the fibre is as shown below :

The structure of a typical secondary coated optical fibre.

The optical fibres were supplied by Standard Telecommunication Laboratories Limited. Different batches of fibre were used in the experimental work. They are summarised in Table 1 below :

Fibre No.	Type	Fibre Dia.	Overall Primary Coating Dia.	Secondary Coating Dia.
237-117P	Step Index	150 μm	210 μm	1 mm
560-207C	Graded Index	105 μm	165 μm	1 mm
731/831-797P	Graded Index	125 μm	185 μm	1 mm

TABLE 1: A Summary of the type of Optical Fibres and their dimensions used in the experimental work.

CHAPTER 2

EXPERIMENTAL

2.1 TENSILE TEST OF OPTICAL FIBRE IN AIR

Fracture stress of glass fibres usually fall far short of their theoretical values. This was explained by Griffith[8] to be due to the existence of microcracks on the glass surface where the stress is concentrated round the tip of such cracks when the material is stressed. Consequently material at the tip begins to part before the mean stress reaches the bond strength of the glass. For this reason it is not surprising to find a wide variability in fracture strength resulting from the statistical variation of the glass surfaces.

Fifty sequential samples of secondary coated optical fibre were stressed to fracture in order that meaningful statistics could be obtained. The gauge length and the strain rate were fixed at 0.5 m and 1.67×10^{-3} s^{-1} respectively to be compatible with previous tensile measurements at Standard Telecommunication Laboratories. Tests were carried out on a bench top Instron tensometer (Model No.1026) and capstan grips were used to support each end of the fibre (Fig.1). The fracture loads on the actual fibres were calculated by subtracting the load carried by the coating from that of the composite. Secondary coated fibres were used in the experimental work because difficulties were encountered in gripping primary coated or bare fibre without any end effects.

2.2 DYNAMIC FATIGUE TEST IN AIR

The strength of optical fibres is known to be time-dependent. This phenomenon commonly known as static fatigue is believed to be due to slow growth of pre-existing surface flaws by a stress corrosion process. Consequently, the strength of the fibre degrades under static as well as dynamic load. In order that long term prediction of optical fibre could be evaluated, the fatigue parameters will have to be obtained.

One method of achieving this is to carry out a dynamic fatigue test.

Tensile tests were conducted with the Instron tensometer at strain rates ranging from 1.19×10^{-1} to 1.19×10^{-4} s^{-1}. The measurements were done in air of about 40% relative humidity and at $20^{o}C$. Twenty samples were tested at each of the four different strain rates chosen. In all the tests the gauge lengths were fixed at 0.07 m. Different strain rates were obtained by varying the cross-head speed of the tensometer. The cross-head speeds chosen were 0.5, 5, 50 and 500 mm min^{-1} which were the widest possible range of speeds obtainable from the tensometer.

2.3 COMBINED TENSION AND TORSION TEST

Optical fibres can be subjected to combined tension and torsional stresses during cabling. Data obtained from combined tension and torsion test would be of great interest to the cable designers.

A method was developed to test similar 0.5 m gauge length optical fibre under combined tension and torsion. The torsion was applied by attaching the bottom grip of the Instron tensometer to a rotating motor at 10 rev.min^{-1}. A predetermined level of torsion was first applied to the fibre, which was then stressed in tension up to its fracture point at a strain rate of 1.67×10^{-2} s^{-1}. Fifty sequential specimens were tested at each level of torsion, which were as follows: 628, 942, 1257 and 1571 rad m^{-1}. The total number of specimens tested totalled 250 specimens. This was thought a reasonable basis for a statistical study.

2.4 COMBINED TENSION AND TORSION TEST AT DIFFERENT TEMPERATURES.

Strength of glass fibre is known to depend not only on the surface state of the fibre but also the subcritical crack growth when the material is stressed. Stress corrosion was believed to be the cause of the subcritical crack

growth and therefore thought to be temperature sensitive.

The tests were done in the same manner as the tension-torsion tests except that the specimens and grips were housed in a temperature cabinet (Instron Model 3111) during the test. The coolant used for low temperature tests was liquid nitrogen.

The samples were subjected to an initial torsion of 628 rad m^{-1} and subsequently pulled to fracture over a temperature range of $-40^{o}C$ to $+50^{o}C$. The gauge length was maintained at 0.2 m in order for the specimen to fit in the temperature cabinet. Test of ten samples was carried out at each temperature at increments of about $20^{o}C$. The temperature range was limited to these values because above this range softening of the polypropylene coating occurred, followed by pull out of the fibre from the jacket. At temperatures below $-40^{o}C$ brittle fracture of the plastic occurred before that of the fibre, which lead to slipping between the plastic and the fibre.

2.5 TENSILE TEST IN DIFFERENT pH VALUES

A container was constructed to adapt to the bottom grip of the Instron tensometer (Fig. 2). This enabled optical fibre to be tested in a variety of solutions.

Secondary coated optical fibre was cut into lengths of about 0.3 m from a reel. Batches of 60 samples were then presoaked in solutions of hydrochloric acid of pH 1.0 and sodium hydroxide of pH 13 for 1½ months to allow complete transfer of ionic electrolytes through the plastic coatings. Half the samples of each batch were tensile tested in the solutions under the same pH values at which they were pre-soaked and the next were dried in an oven at $40^{o}C$ for 4 days and tested in laboratory environment. Again tensile tests were conducted on the Instron 1026 at a crosshead speed of 20 mm min^{-1} over a gauge length of 0.2 m corresponding to a strain rate of 1.67×10^{-2} s^{-1}.

2.6 DYNAMIC FATIGUE TEST IN DIFFERENT pH VALUES.

In view of the weakening effect of the optical fibre, observed when tested in alkaline environment, it was thought worthwhile to investigate the dynamic fatigue effect of the fibre in different ionic solution of different pH values.

These tests would provide fatigue parameters for long-term strength predictions and sub-critical crack growth under such environments.

Different batches of optical fibres were presoaked in distilled water and solutions of hydrochloric acid and sodium hydroxide of different strengths for 1½ months to allow complete ionic diffusion through the coatings. The concentrations of the hydrochloric acid in which the fibres were presoaked were 0.1N, 1,0N and 5.ON. Each batch of the fibres were tested at different strain rates by varying the crosshead speed of the tensometer. Twenty samples were tested at each of the strain rates. The strain rates chosen were 1.19×10^{-1}, 1.19×10^{-2}, 1.19×10^{-3}, 1.19×10^{-4} s^{-1}.

2.7 SCANNING ELECTRON MICROSCOPE ANALYSIS OF FRACTURE SURFACES.

Brittle failure often leaves behind fracture markings. These markings can reveal the origin of the fracture and the direction from which it propagates. Therefore, fracture of optical fibre under various loading conditions can be understood by examining its fracture surface.

Optical microscopes could not provide the necessary resolution and depth of focus for the study of fracture surfaces of optical fibres. Therefore a scanning electron microscope had to be employed. The scanning electron microscope used was an ISI SUPER III A.

The Optical fibre being non-conducting had to be coated with gold. This was necessary to prevent charging effect when the electron beam of the microscope scans across the sample.

Four samples were mounted on a stub as shown in Fig.(3). Silver dag was then applied between the stub and the base of the sample so that good electrical contact could be achieved. The samples and stub were then coated with gold with a sputter coater unit (Polaron ES 100). The optimum coating condition were found to be 2.5 kV and 20 mA for about 1½ minutes.

CHAPTER 3

RESULTS

3.1 TENSILE TESTS OF OPTICAL FIBRE IN AIR

The probability of failure of optical fibre of a given length has been found to be well described by the Weibull distributions [9]. The probability of failure F(x) is expressed by the function :

$$F(x) = 1 - \exp\left(-\left(\frac{\sigma_f}{\eta}\right)^{\beta}\right) \quad \ldots\ldots 3.1.1$$

where σ_f is the fracture stress and η and β are constants.

Weibull probability graph paper with ordinate $\ln \ln\left(\frac{1}{1 - F(x)}\right)$ and abscissa $\ln \sigma_f$ was used to plot the fracture stresses obtained from the tensile tests as shown in Fig. (4). The graph showed three distinct regions. About 90% of the specimens fell in the upper end of the curve, 5% in the plateau region and 5% in the lower end.

Fractographic analysis of the weaker specimens corresponding to the lower end of the Weibull plot revealed markings typically that of a brittle failure, as seen in Fig.(5). Three different regions were visible. These regions were (1) the mirror (a flat, smooth region), bounded by (2) the onset of mist (a region of small ridges), which was bounded, in turn by (3) the hackle (a region of larger ridges), as indicated in Fig.(6). The origin of fracture of these weak specimens were predominantly from the surface of the fibre. The 'inner' mirror size (r_i) which was the radius bounded by the mirror region before the onset of the mist region was estimated to be about 3.25 μm Fig. (6).

Internal flaws (Fig.7) were observed from specimens in the 'plateau' region of the Weibull curve. At the upper end of the curve, the fracture origin could not be determined

from the fractograph. This is due to the release of a large amount of strain energy during the fracture process thus shattering the fracture surfaces.

3.2 DYNAMIC FATIGUE TEST IN AIR

It has been demonstrated by Wiederhorn[10] that a good representation of subcritical crack growth in glasses is given by

$$V = AK_I^N \qquad \ldots\ldots \quad 3.2.1$$

where V is the subcritical crack velocity, K_I the stress intensity factor and A and N are constants that depend on environment and material composition.

Based on the assumption that failure of glass occurs from stress dependent growth of pre-existing flaws to dimensions critical for spontaneous crack propagation, it can be derived from equation 3.2.1. that

$$\sigma_f^{N+1} = \left(\frac{2}{AY^2 (N-2) K_{IC}^{N-2}}\right) (N+1)E \ \sigma_{IC}^{N-2} \dot{\epsilon} \quad ..3.2.2.$$

where σ_f = fracture stress, $\dot{\epsilon}$ = strain rate, K_{IC} = critical stress intensity factor, Y = geometric constant, E = Young's Modulus and σ_{IC} = fracture stress in inert environment.

If $\left(\frac{2}{AY^2 (N-2) K_{IC}^{N-2}}\right) = B$

then $\log \sigma_f = \frac{1}{N+1} (\log B + \log (N+1) + (N-2) \log \sigma_{IC} + \log E + \log \dot{\epsilon})$ $\ldots\ldots$ 3.2.3

A graph of $\log \sigma_f$ verus $\log \dot{\epsilon}$ was plotted for secondary coated optical fibres tested in air at 20°C and 40% relative humidity (Fig.8). From linear regression analysis of $\log \sigma_f$ vs $\log \dot{\epsilon}$, the slope $\frac{1}{N+1} = 0.0375$ corresponding to a value for N of 25.7. The intercept $\frac{1}{N+1} (\log B + \log (N+1) + (N-2) \log \sigma_{IC} + \log E) = 9.81$ ... 3.2.4.

Using the averaged inert strength of optical fibre as measured in liquid nitrogen temperature where fatigue is thought does not exist, σ_{IC} was found to be 12.6×10^9 Nm^{-2} (11). From this value of σ_{IC}, log B was found to be 10.28.

It can also be derived from equation 3.2.1 that the time to failure (t_f), under a constant applied stress (σ_a) due to subcritical crack growth, is

$$t_f = B \quad \sigma_{IC}^{N-2} \cdot \sigma_a^{-N} \qquad \ldots\ldots 3.2.5$$

hence $$\log t_f = \log B + (N-2) \log \sigma_{IC} - N \log \sigma_a \ldots 3.2.6$$

substituting N = 25.7 and log B = 10.28 into equation 3.2.6

$$\log t_f = 10.28 + 23.7 \log \sigma_{IC} - 25.7 \log \quad a \ldots 3.2.7$$

Having shown a time to failure relationship with applied stress value, it would be worthwhile in the context of the optical fibre industry to link this relationship with failure statistics. The inert strength distribution of these optical fibres can be reasonably assumed to be given by Weibull distribution as mentioned earlier, hence

$$\log \ln \frac{1}{1-F(x)} = \beta \log \frac{\sigma_{IC}}{\eta} \qquad \ldots 3.1.1.$$

Assuming $\beta = 16$ i.e. to be the same as that in air at room temperature (Fig.9) and $\eta = 12.73 \times 10^9$ Nm^{-2}, then equation 3.1.1 becomes

$$\log \ln \frac{1}{1-F(x)} = 16 \log (\sigma_{IC}/12.73 \times 10^9) \qquad \ldots.3.2.8.$$

The minimum time to failure after proof testing is given by (10)

$$t_{min} = B \left(\frac{\sigma_p}{\sigma_a}\right)^{N-2} \cdot \frac{1}{\sigma_a} \qquad \ldots\ldots 3.2.9$$

where σ_p = proof stress. Using log B = 10.28 and N = 25.7 then

$$\log t_{min} = 10.28 + 23.7 \log (\sigma_p/\sigma_a) - 2 \log \sigma_a \ldots 3.2.10$$

Substituting $\log \sigma_{IC}$ from equation 2.2.8 into equation 3.2.6

$$\log t_f = 249.8 + \frac{23.7}{16} \log \ln \left(\frac{1}{1-F(x)}\right) - 25.7 \log \sigma_a \qquad \ldots 3.2.11$$

A design diagram based on dynamic fatigue data given in the preceeding section where B = 10.28 and N = 25.7 is given in Fig. (10). The lines that run from left to right relate the minimum failure time after proof testing to the applied stress (equation 3.2.10), where the number over each end of the line gives the ratio (σ_p / σ_a). Superimposed on the diagram is the failure probability without proof testing (equation 3.2.11).

3.3 COMBINED TENSION AND TORSION TEST

The data for various combinations of tension and torsion were plotted into Weibull curves in Fig. (11) and Fig.(12). In pure tension and three other different levels of torsion, severely flawed specimens were observed as depicted by the presence of a 'tail' in the Weibull curves. At the lowest torsion level of 625 rad m^{-1}, there were no badly flawed specimens, therefore a single straight line was obtained on the Weibull plot.

Successive fracture stress of each sample from the reel of fibre were plotted in Fig. (13). There was a strong tendency for weak samples to fall very close to each other, indicating that larger flaw population was distributed over relatively short sections of the fibre.

Decreasing tensile strengths were observed as increasing levels of torsion were applied to the optical fibre. (Fig.14). This figure also shows that the degree of scatter increases with levels of torsional stress. This is also evidenced by a decrease in the slope of the Weibull curves as the levels of torsion were increased, indicating a greater spread of strength.

3.4 TENSION AND TORSION TEST AT DIFFERENT TEMPERATURES.

The averaged maximum principal stress of the ten tests was plotted against temperature as shown in Fig. (15). Severely flawed samples were excluded from the analysis. Over the range -20°C to 50°C the strength remained fairly constant at

a maximum principal stress of about 3.3×10^9 Nm^{-2}. There was a gradual increase in strength below $-20^{\circ}C$.

3.5 TENSILE TEST IN DIFFERENT pH VALUES

Weibull curves of tensile strength in pH 1 and pH 13 were plotted in Fig. (16). Results showed that fibres presoaked and tested in pH 1 and pH 13 were both weaker than those stored and tested in the normal laboratory environment. Fibres were stronger at a pH of 1 than those at pH 13.

Table 2 showed the mean tensile strength and percentage strain of the fibres tested in the different pH conditions. The badly flawed specimens were excluded in this analysis. The mean strength of the fibres presoaked and tested in pH 1 and pH 13 showed a fall in strength of 4% and 4.5% respectively, as compared with those tested in laboratory conditions. Since the number of specimens tested were large this could not be due to experimental error. The difference between the strength measured in pH 1 and pH 13 was about 6%.

The loss of fracture stress level of the presoaked fibres was shown to be completely recoverable after drying in oven at $40^{\circ}C$ for 4 days, as indicated in Table (2).

3.6 DYNAMIC FATIGUE TEST IN DIFFERENT pH VALUES

Log-log graphs of fracture stress against strain rate of secondary coated optical fibre, for different acidic and alkaline environments, are given in Fig.(17,a,b,c,d,e,f). The slopes of each graph were obtained by linear regression. From the slopes of the graphs the stress corrosion susceptibilities (N) for the various environments were calculated in the same manner as in Chapter 3.2. The results obtained are summarised in Table 3.

	TS GN/m^2	CV	% strain
TS average stored at Lab. atmosphere GN/m^2	3.68	8.7%	5.04
Presoaked and tested in HCl of pH 1.0.	3.54	4.6%	4.85
Presoaked and tested in NaOH of pH 13.	3.33	3.7%	4.56
Presoaked in HCl. Dried in oven and tested in lab.atmosphere.	3.62	3.9%	4.96
Presoaked in NaOH, dried in oven and tested in lab. atmosphere.	3.68	4.9%	5.04

TS = tensile strength
CV = coefficient of variance

TABLE 2: The mean tensile strength and percentage strain at different environmental conditions.

Environmental Conditions	Slope $\left(\frac{1}{N+1}\right)$	Stress Corrosion Susceptibility (N)
5.0 N NaOH	0.0500	19.0
1.0 N NaOH	0.0485	19.5
0.1 N NaOH	0.0416	23.0
DISTILLED WATER	0.0405	23.5
0.1 N HCl	0.0375	25.5
1.0 N HCl	0.0339	28.5

TABLE 3: A summary of Stress Corrosion susceptibilities in both Acidic and Alkaline Environments.

The stress corrosion susceptibility (N) of optical fibre in dstilled water obtained by dynamic fatigue was 23.5. This value falls to about 19.0 under sodium hydroxide solution of 5.0 N and increases to about 28.5 under hydrochloric acid of 1.0 N.

DISCUSSIONS

4.1 THE TENSILE STRENGTH OF OPTICAL FIBRE

The variability of tensile strength of apparently identical samples of optical fibres tested is explained in terms of Griffith microcrack hypothesis[8]. Microcracks or flaws on the surface or within the bulk of the specimens act to concentrate applied stress to values which would locally exceed the theoretical strength of the glass and permit crack propagation. The observed strength is largely dependent upon the size of the flaws present in each of the samples tested. Variation on the sizes of flaws present in the fibre would, therefore, lead to a statistical variation in tensile strength.

A typical Weibull curve, Fig.(14) from the tensile tests did not produce a simple straight line. The presence of a 'tail' at the lower end of the curve is observed. This suggests different flaw populations existing on the fibre which were generated from different sources.

The large surface flaws which predominated at the weaker end of the Weibull curve are of particular interest. Potentially these are the flaws that may lead to fracture during cabling and service. Particles of dust in the pulling environment are believed to be the prime source of these large flaws[12]. These particles which stick to the hot glass surface can generate flaws as the glass is cooled due to differential thermal expansion between the particles and the glass matrix.

The strength of long lengths of optical fibre would be determined by the presence of the large surface flaws, as found in the tensile test of large samples of 0.5 m gauge lengths. Of the limited samples with large flaws obtained from the entire tensile tests a Weibull chart was plotted in Fig.(18). The straight line drawn through

the points is characterised by a slope β of about 5 and η of 1.67×10^9 Nm^{-2}. From a total length of 60m in 0.5 m gauge length samples tested, thirteen of these weak samples were found. This is equivalent to a flaw density of about one in every 5 m length, assuming there was only one severe flaw in each sample.

Fracture mechanics could be applied to predict critical flaw sizes, which, in turn, could be correlated to the different flaw populations found in the optical fibres. The relationships used are as follows[13] :-

$$C_{crit} = \frac{Z^2 K_{IC}^2}{2 \sigma_f^2} \qquad \ldots.4.1.1.$$

The equation assumed a semi-elliptical shape flaw where C_{crit} is the critical flaw size, K_{IC} the critical stress intensity factor , σ_f the nominal failure stress and Z a constant which depends on flaw geometry. Wiederhorn et al[14] in studying the subcritical crack growth of glass in vacuum of fused silica obtained a value of 0.74 MN $m^{-\frac{1}{2}}$ for K_{IC}. At the time of fracture, the flaw usually approximates a semi circular shape as illustrated from the fractograph (Fig.6). Based on this assumption a value of 1.12 is calculated for Z. The critical flaw size C_{crit} can then be correlated to the fracture stress σ_f, as shown in Fig. (19). Fracture stress, at about 1.3 GNm^{-2} corresponds to large surface flaw sizes of about 0.2 μm; whereas bulk flaws are of the order of 0.1 μm. The high strength observed at the upper end of the Weibull curve indicates a critical flaw size of 0.03 μm for this region.

Melcholsky et al[15] showed that the product of strength and square root of the inner mirror size is a constant which they refer to as the inner mirror constant

$$\sigma_f \quad r_i^{\frac{1}{2}} = Ai \qquad \ldots.4.1.2$$

where r_i is the inner mirror radius and Ai is the inner

mirror constant. From the weak specimens, the inner mirror constant Ai was calculated to be 2.24 MN $m^{-3/2}$. Thus the fracture stress of the fibre can be estimated by measuring the mirror size in the fracture.

Furthermore, by substituting σ_f in equation (4.1.2) with equation (4.1.1), the following relationship can be obtained :

$$\frac{r_i}{c_{crit}} = \frac{2\,Ai^2}{Z^2\,K_{IC}{}^2} \qquad \ldots\ldots\ 4.1.3.$$

From equation (4.1.3) the inner mirror to critical flaw size ratio (r_i/c_{crit}) is a constant - estimated to be about 14.5. Re-writing equation (4.13) $r_i = C_{crit} \times$ const., for optical fibre $r_i = 14.5\ C_{crit}$. Therefore, for a given mirror size, the flaw size could be evaluated. For example, the specimen that failed at 1.24 GN m^{-2} (Fig.6), the flaw size estimated from the mirror size was 0.22 μm, and by using equation (4.1.1) the flaw size was calculated to be 0.25 μm (Fig.19). The mirror size measurement could, therefore, be used to determine critical flaw size, particularly the large one, quite accurately ranging from strength values of between approximately 0.18 GN m^{-2} to about 2.0 GN m^{-2}. This technique could be used in predicting flaw size of optical fibre which failed during fabrication or proof stressing where the actual failure stress is usually unknown.

The internal flaws were probably due to the chemical discontinuity inherent within the cross-section of the fibre. This source of flaws could originate from imperfect vapour deposition or during the collapsing stage of the preform. Flaws generated were carried through by the pulling process.

The high strength observed in the upper end of the Weibull curve is believed to be due to numerous minute surface

flaws existing on the preform which were subsequently carried through during the pulling process. This is evidenced by a substantial increase in strength by fire polishing the preform before the fibre is pulled, as found by Shonhorn et al[16]. Further improvement in strength was observed if the preform was fibre polished and pulled by a laser puller, which produced very high surface temperature on the preform.

4.2 DYNAMIC FATIGUE TEST IN AIR

In the design of optical fibre cable, an important consideration is its long term mechanical reliability. It is, therefore, necessary to take into account not only the wide variability in fracture strength, but also the subcritical crack growth characteristics when the fibre is subjected to a residual mechanical stress.

Long term mechanical reliability can be assured by proof testing whereby the components are subjected to stresses that are greater than those expected in service to eliminate the weak components. In this way, the fibre that survives the proof testing will have a minimum lifetime, as predicted by equation 3.2.9. provided no crack growth takes place during unloading. For proof testing to be effective, it should, therefore, be conducted under relatively inert environment with rapid unloading rates.

Design diagrams for optical fibres are constructed to decide if proof testing is necessary, and, if so, the required proof stress necessary to assure a certain lifetime. The diagram obtained (Fig. 10) was based on dynamic fatigue and the failure probability curves were obtained from 0.5m gauge length tensile tests. It must be remembered that the severely flawed samples were excluded in the analysis. In practice the optical fibre used in a cable are much longer compared to the tested gauge length. By using a factor to take into account of the size effect using Weibull statistics

a design diagram was obtained for a kilometre length fibre as shown in Fig. (20).

The design diagram can be used in the following manner. If the optical fibre is to operate under a stress of 1 GNm^{-2} for 25 years, the failure probability without proof testing would be 1.3×10^{-3} or 0.13%, as indicated at the point of intersection in Fig. (20). Typically, the residual strain found in cabled optical fibre is within 0.25% compressive to 0.5% strain[17]. The design diagram indicates that at these stress levels, the failure probability is extremely low, hence proof testing appeared to be quite unnecessary. It should be noted that the large flaws were excluded in the analysis, therefore only if these flaws can be eliminated, will the fibres be safe without proof testing.

Results from the tensile test in the previous section showed presence of relatively large surface flaws. By using Weibull failure statistics of these flaws (Fig.18), a design diagram was obtained as given in Fig. (21). If a typical value of 0.2% strain (0.14 GNm^{-2}) is taken as the residual strain of the fibre in the cable and 25 years service life is assumed, then 0.002% of the large flaws would fail if proof testing is not conducted, as indicated from the design diagram. To assure no failures, a proof stress ratio of 4.26 will be required corresponding to a proof stress of 0.6 GNm^{-2}. Design diagram can also be used to predict failure rates during proof testing. For example, a proof stress of 0.6 GNm^{-2} conducted under the same environmental conditions for 1 second would result in the percentage failure of the large flaws of about 0.08%.

4.3 STRENGTH OF OPTICAL FIBRE UNDER COMBINED TENSION AND TORSION.

Large surface flaws which resulted in low strength were mainly attributed to contamination of particles on the fibre surface, as discussed in section 4.1. These flaws can be generated either from the dust in the pulling environment or

the pulling environment of the preform rod. The tendency for the large flaws to occur close together along the fibre as observed in the tests suggested localised contamination of the rod would result in flaws distributed over a relatively short section.

Another possible cause could be due to dust particles adhering on the surface of the fibre over a short section. This could happen if there was an intermittent draft in the vicinity of the pulling environment leading to dust particles settling over a short section of the fibre while the fibre was being pulled.

The state of stress on the fibre subjected to combined tension and torsion can be described by the two principal stresses σ_1, and σ_2

$$\sigma_1, \sigma_2 = \frac{\sigma_y}{2} \pm \left[\left(\frac{\sigma_y}{2} \right)^2 + \tau_{xy}^2 \right]^{\frac{1}{2}} \quad \ldots 4.3.1$$

where σ_y = tensile stress and τ_{xy} = torsional shear.
If maximum principal stress σ_1 can be assumed to be the component contributing to the initiation and propagation of the flaws, then the above equation predicts a decrease in applied axial stress with an increase in torsion.
This effect was seen in Fig. (11) and Fig. (12). Torsional stress can, therefore, have a serious detrimental effect in that it is very liable to increase the probability of failure of optical fibres in a cable.

One of the main objectives in the study of failure of optical fibre in combined stresses is to determine how the strength compares with pure tensile strength. Table 3 below shows the state of stresses of fracture for various combination of tension and torsion on the surface of the component in terms of principal stresses. Each set of values represented an average of about 50 samples, the badly flawed samples were excluded.

Angle of Twist (rm^{-1})	0	628	942	1257	1571
σ_1, GN m^{-2}	4.99	4.64	4.59	4.28	4.19
σ_2, GN m^{-2}	0	-0.23	-0.52	-0.99	-1.58

TABLE 4: The mean principal stresses at fracture at various angle and twist.

It is interesting to see from the table that with increasing torsion, the maximum principle stress σ_1 decreases significantly compared with uniaxial tensile strength. Equation 4.3.1 is, therefore, not strictly applicable in predicting the fracture strength subjected to combined stresses. As tests at higher torsional levels took longer, some losses in strength could be attributed to a contribution from static fatigue,but this could not account for all the loss as observed in the tests.

Statistical theory of failure based on randomly distributed flaws suggests an increase in maximum principle stress under combined tension and torsion which further conflicted the data. This can be visualised by taking the case of a specimen subjected to idealised 'eqi' biaxial tension stress. Under this stress system the number of flaws would likely to propagate are more than the case of uniaxial tensile stress dependent on the directional distribution of the flaws. Consequently, uniaxial strength would be higher than that of 'equi' biaxial stress. Conversely, a 'tensile/compression' state of stress as realised in a tension/torsion test would result in increase in strength compared with uniaxial stress as the number of operative flaws that are likely to lead to failure is reduced.

The effect of the loss in maximum principal stress with increasing torsion can be explained in terms of orientation of flaws of the fibre. The preform flaws could be elongated

along the fibre axis when drawn down to fibre. These elongated flaws are not so critical to uniaxial tensile stress. Under a combined tension and torsion, the plane of the maximum principal stress moves away from the plane perpendicular to the fibre axis and, therefore, becomes more critical to the flaws. With increasing torsion, the plane of principal stress becomes even more critical and hence a reduction in strength was observed. This might also account for the decrease in Weibull slope as torsional stress was increased.

There were insufficient data on the weak samples for thorough analysis to be carried out. Fractographic analyses of those specimens showed fractures initiating from both the bulk as well as the surface of the fibre (Fig. 22 and Fig. 23). Surface flaws,as previously discussed, were thought to be caused by poor handling of the preform or the presence of dusts in the pulling environment, whereas bulk flaws were probably due to chemical discontinuity inherent over the cross-section of the fibre.

4.4 TENSION AND TORSION TEST AT DIFFERENT TEMPERATURES.

Brittle fracture in glasses is known to be not only stress but time dependent. This is attributed mainly to sub-critical crack growth by a stress corrosion process in the presence of water[18]. It was thought that for a stress corrosion process, the important parameters that would control the crack growth are the temperature and the partial pressure of water if it is in gaseous state.

The effect of increasing temperature would be generally to increase the reaction rate between the silica and water and, the increased mobility of the water molecules will enhance the crack propagation rate, thus reducing the strength. This effect was not served over the temperature range of $-20^{o}C$ to $50^{o}C$. The constancy over this temperature range is attributed to the fall in the availability of adsorbed

water as the temperature increases[18]. This resulted in an increase in strength thus compensating for the strength lost due to increased mobility of water molecules and water/ silica reaction rate.

The increase in strength below -20°C can be accounted for by the reduction in the amount of water present. Cooling effect and low humidity environment resulting from using liquid nitrogen as coolant contribute to the low availability of water.

Proctor et al[18] showed that fused silica fibre strength actually increased over the temperature range of 0 - 200°C. They attributed this effect to the loss of water on the surface of the fibre to be the most important factor and that temperature had little effect on the strength to account for the increased strength observed.

Duncan et al[11] in testing bare optical fibres under low temperature and varying humidity showed a steady increase in strength as temperature was lowered and achieved a strength of 12.6 GNm^{-2} at liquid nitrogen temperature. They also showed that similar increase in strength could be achieved by testing under a very dry environment at room temperature. It was concluded that strength in silica fibre is relatively temperature insensitive but is determined mainly by the amount of water present in the environment.

4.5 TENSILE TEST IN DIFFERENT pH VALUES

The shape of the Weibull curves under different pH values could be explained by the presence of different flaw poluations as discussed in section 4.1. The weaker end of the curves were dominated by the surface flaws and the intermediate strength by internal flaws.

Compared to the specimens tested under normal laboratory conditions, presoaked fibres showed a reduction in strength in both highly acidic and alkaline solutions. This again

suggests that the availability of water in the environment is the predominant factor in determining the subcritical crack growth and hence the strength of the fibre. The higher strengths observed in air compared to those in aqueous solutions is mainly due to the relatively dry environment in which they were tested. The abundance of water present in solution acted to increase the crack growth of the flaws thus contributing to the reduction in strength.

In solutions, the fibre was observed to be stronger in acidic rather than alkaline environment. This weakening effect in alkaline solution is believed to be due to the presence of hydroxyl ions in the solution which modified the subcritical crack growth[7]. The effect of hydroxyl ions is thought to aid in the stress corrosion process at the crack tip thus resulting in weakening the fibre. On the other hand the lack of hydroxyl ions in acidic environment lead to an increase in its tensile strength of value somewhat

When the fibre was dried after presoaking, the amount of water adsorbed on the fibre surface would decrease thus contributing to the increase in strength observed.

Presoaking in either acidic or alkaline environment did not appear to permanently weaken or strength the fibre when dried. The active hydroxyl ions in solution became rather inactive as sodium hydroxide after undergoing the drying process and therefore would have little effect on the strength. The fibre strength after presoaking and drying reverted to its dependence on the availability of water present in its immediate environment.

4.6 DYNAMIC FATIGUE TEST IN DIFFERENT pH VALUES

Subcritical crack growth of fused silica under different environmental conditions can be studied from three types of experiments namely crack velocity, static fatigue and dynamic

fatigue. Wiederhorn and Johnson[19] have evaluated the effect of electrolyte pH on the crack propagation of silica by the crack velocity technique. Although this technique has provided fundamental information regarding subcritical crack growth, it may not be relevant to optical fibre mainly because the defects found on these components are quite different from the cracks induced onto the crack velocity specimens. Dynamic fatigue technique was, therefore,adopted as it could be carried out on the Instron Tensometer with some modifications.

Stress corrosion susceptibility (N) of secondary coated optical fibres in distilled water found by dyanamic fatigue was compatible with the value of 22 obtained by W J Duncan et al[10]. The general trend in that stress corrosion susceptibilities are higher in acidic and lower in alkaline solutions agreed with the results obtained by Wiederhorn although the magnitudes are not the same. This could be due to the fact that crack velocity experiment uses macrocracks whereas in optical fibres the cracks are usually much smaller. In addition, plastic coating surrounding the fibres may act to inhibit the ion transport to the crack tip thus affecting the stress corrosion rate.

CONCLUSIONS

Three different flaw populations were found to exist in a typical length of optical fibre. Large surface flaws operated at strength values of about 0.5 GN m^{-2}. The origin of which was believed to be due to surface contamination of the preform rods or the presence of dust in the pulling environment. Internal flaws were mainly responsible for failure strength of between 2 GN m^{-2} to 3 GN m^{-2}. This was caused by a build-up of stress during the chemical vapour deposition process. The high strength values of around 3.5 GN m^{-2} to 5.0 GN m^{-2} were thought to be due to numerous minute inherent flaws that are characteristic of the pulled fibre surface.

The general expression obtained from fracture mechanics (i.e. $c = \frac{Z^2 K_{IC}}{2 \sigma_f^2}$ 4.1.1) was used to calculate flaw sizes. The origin of fracture in optical fibre particularly the the large surface flaws and internal flaws, could be located from the electron microscope fractographs. In addition, fractographic analysis was used to estimate flaw sizes especially the larger ones which were of particular interest. The inner mirror size measured from the fractograph to flaw size was found to be about 14.5. This technique was limited to strength values of between 0.18 GN m^{-2} to 2.0 GN m^{-2} above which the mirror was not observed and below which the mirror would extend over the entire fracture surface of the fibre.

Tensile strength of optical fibre was found to increase with increasing strain rates. Stress corrosion susceptibility factor (N) was obtained from dynamic fatigue experiments at 20°C and 40% relative humidity. Under this environment a value of N = 26 was obtained which is compatible with results others determined by static fatigue experiments.

Dynamic fatigue studies are therefore a useful technique for evaluating the subcritical crack growth in optical fibres.

Optical fibre in a typical cable can be subjected to stress values between 0.25% compressive strain and 0.5% tensile strain. Design diagrams constructed for an environment which related probability of failure, time to failure and operating stress of the optical fibre, indicated that if large surface flaws were eliminated, the failure probability was very low. For a typical value of 0.2% strain (0.14 GN m^{-2}) subjected to the fibre in a cable and 25 years of service life, 0.002% of the large flaws would fail if proof test was not conducted. To assure no failure under this service constraint the proof stress required was 0.6 GN m^{-2}.

In testing optical fibres under combined tension and torsion, large flaws were found to be close to each other. This suggested that the preform rod used to produce the fibre was either contaminated locally or there was an intermittent draught in the vicinity of the pulling environment causing dust to adhere over short sections of the fibre.

When the optical fibres were subjected to combined tension and torsion, the strength was found to decrease as the plane of maximum tensile stress was moved away from the plane perpendicular to the fibre axis. This suggested that the flaws were elongated along the fibre axis during the pulling process. The orientation of these flaws was not very sensitive to tensile stress but much more critical to combined tension and torsion. The maximum principal stress obtained by two dimensional stress analysis

(i.e. $\sigma_1 = \frac{\sigma_y}{2} \pm \left[\left(\frac{\sigma_y}{2}\right)^2 + \tau_{xy}^2 \right]^{1/2}$ 4.3.1

cannot fully describe the strength of the fibre when

subjected to combined tension and torsion.

Tensile strength of secondary coated fibre remained relatively constant in the temperature range of -20°C to 50°C. There was a gradual increase in strength below -20°C. Strength of the fibre was thought to be relatively temperature insensitive but much more sensitive to the availability of water in the environment. The increase in strength below -20°C was mainly due to the loss of available water on the fibre surface by the cooling effect. The testing temperature was constrained to -40°C to 50°C below this range brittle fracture of the plastic coating occurred before the fibre leading to fibre pull-out from the coating. Above 50°C necking of the polypropylene coating occurred before the fibre fractured hence the strength could not be accurately determined.

Optical fibre presoaked and tested in acidic environment was found to have higher strengths than in alkaline environment. The presoaked fibre both in acidic and alkaline solutions when dried did not suffer any permanent damage compared to those stored in air environment.

The stress corrosion susceptibilities factor increased with decreasing concentration of OH^- ions. Presence of OH^- ions was believed to contribute to the increased subcritical crack growth rate thus resulting in a lower stress corrosion susceptibility value in alkaline environment compared to that in acidic environment.

FIGURE 1: INSTRON TENSOMETER WITH CAPSTAN GRIPS

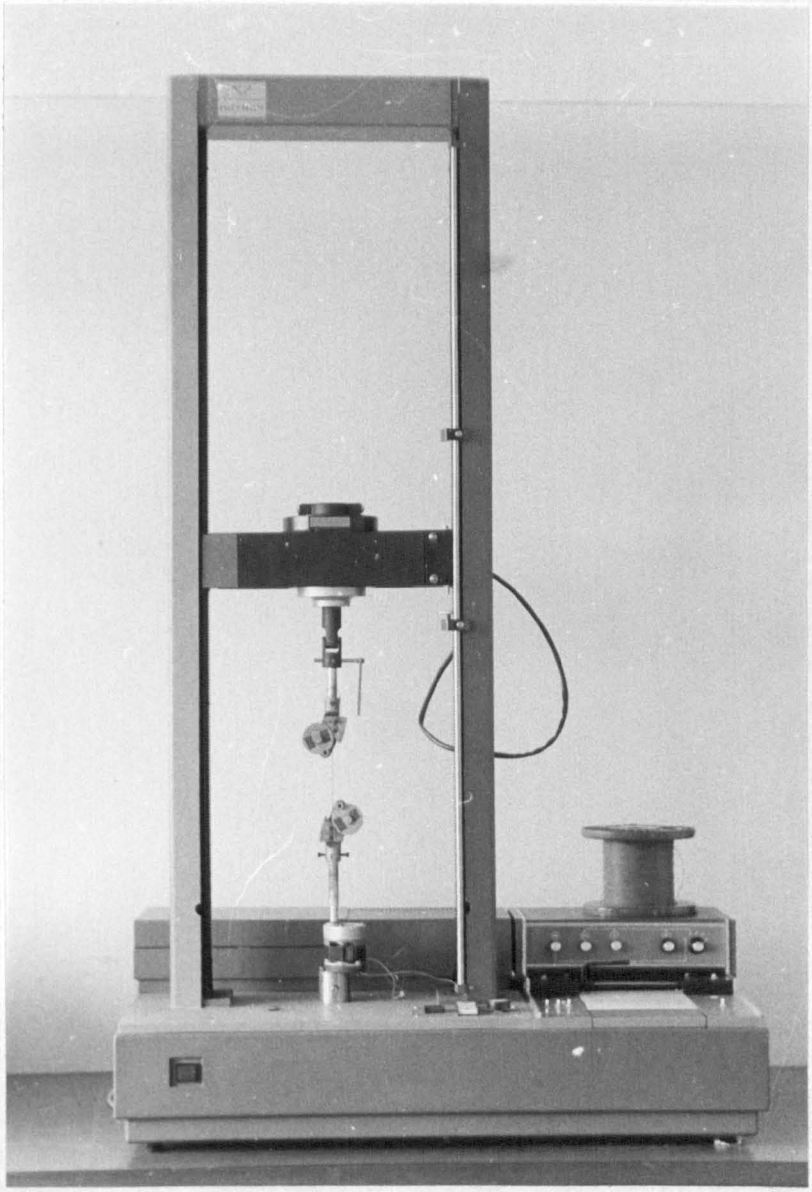

FIGURE 2: INSTRON TENSOMETER CONFIGURATION FOR TENSILE TESTING IN SOLUTIONS.

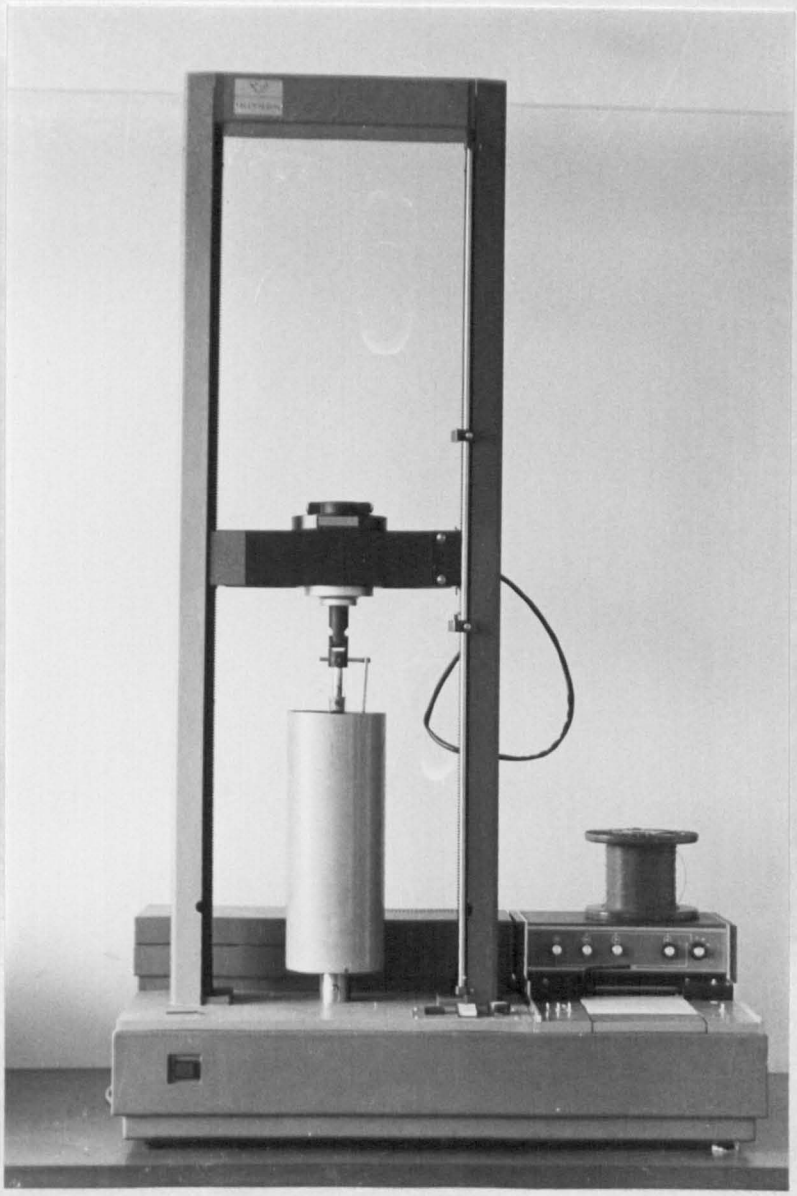

FIGURE 3: (A) CAPSTAN GRIP USED FOR TENSILE TESTING.

(B) OPTICAL FIBRE SAMPLES MOUNTED ON ALUMINIUM STUB AND COATED WITH GOLD.

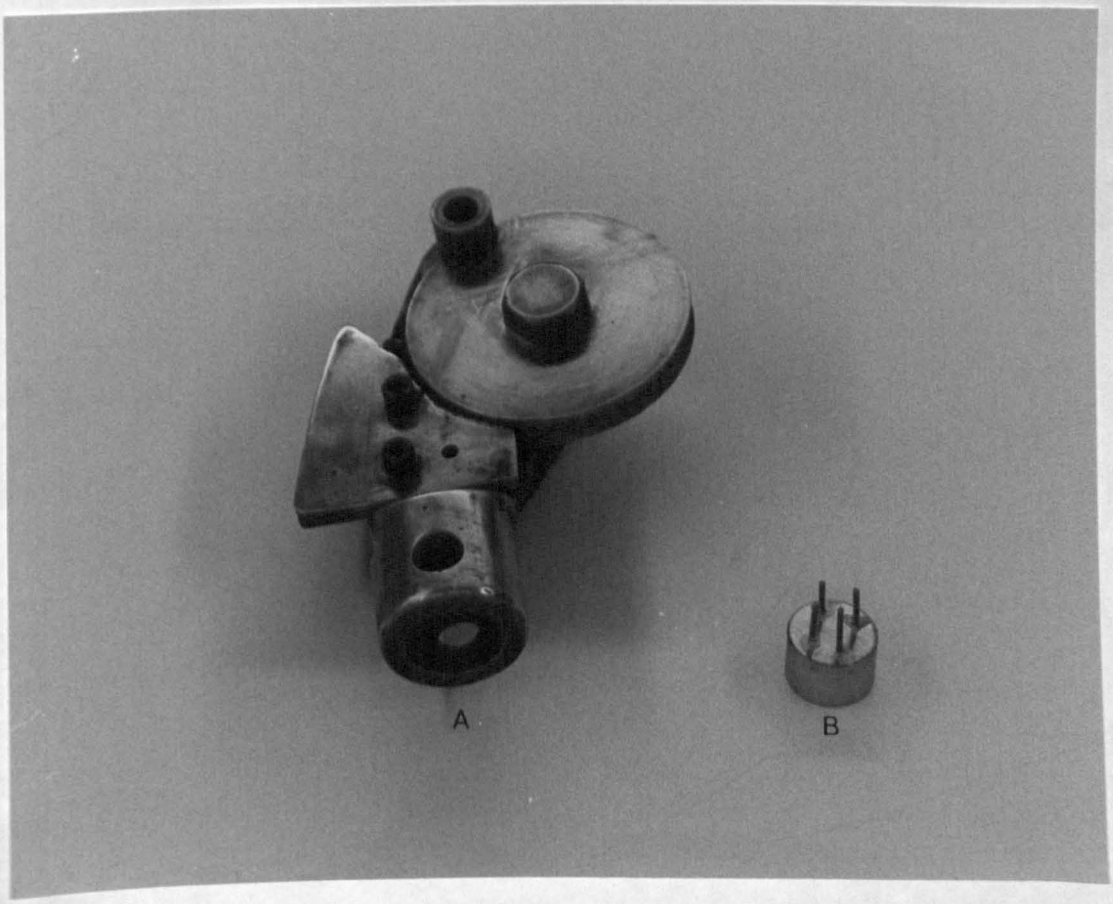

FIGURE 4

WEIBULL PROBABILITY FAILURE PLOTS OF FRACTURE STRESS

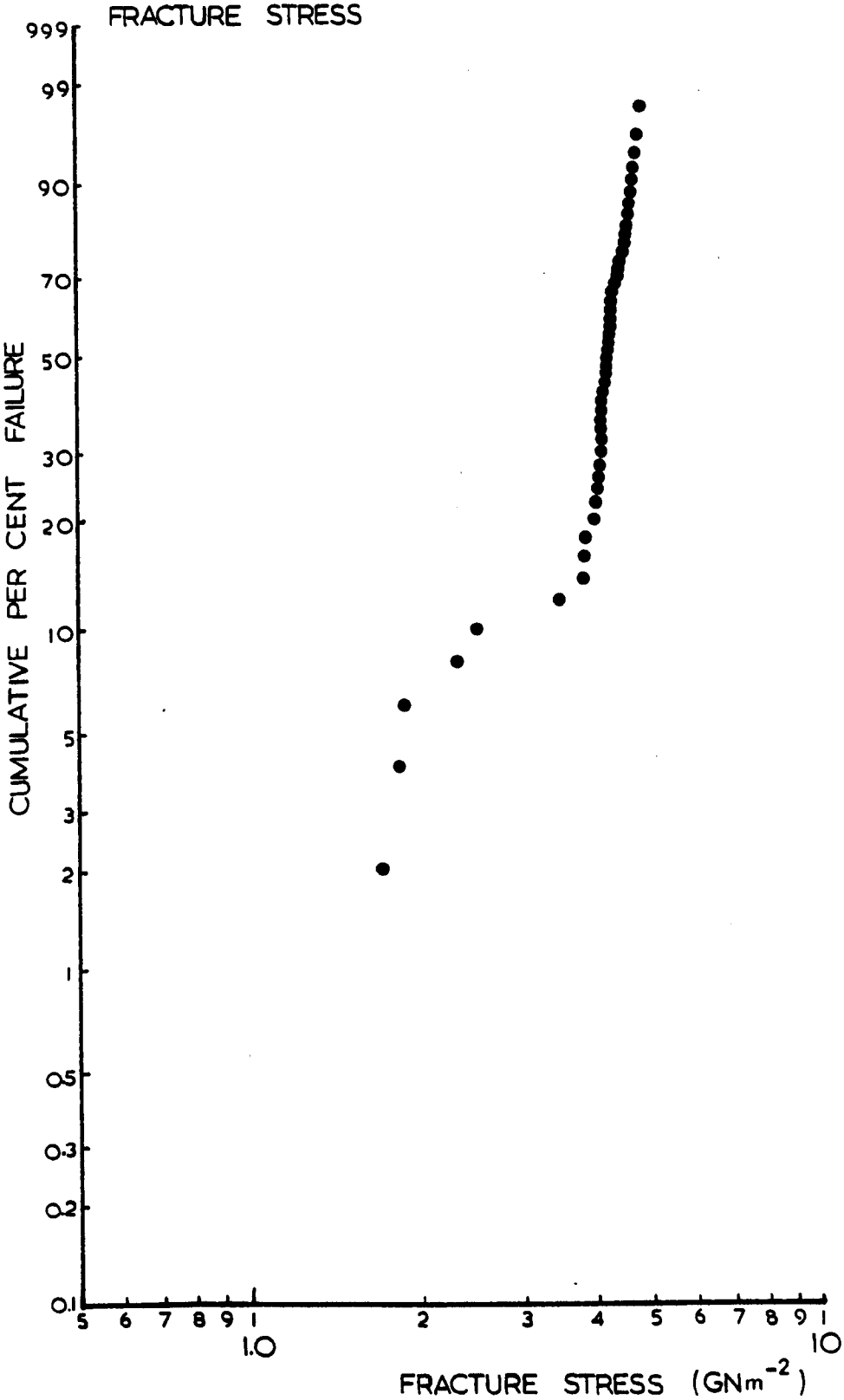

FIGURE 5: A typical SEM fractograph of a weak sample showing fracture originating on the surface. (600 x)

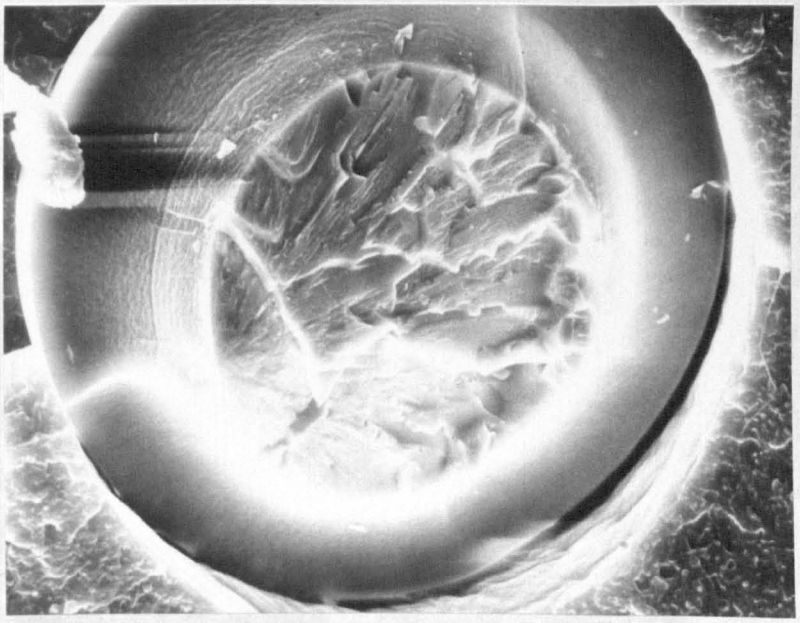

FIGURE 6: The SEM micrograph of the fracture origin showing (a) the mirror (b) mist (c) hackle.

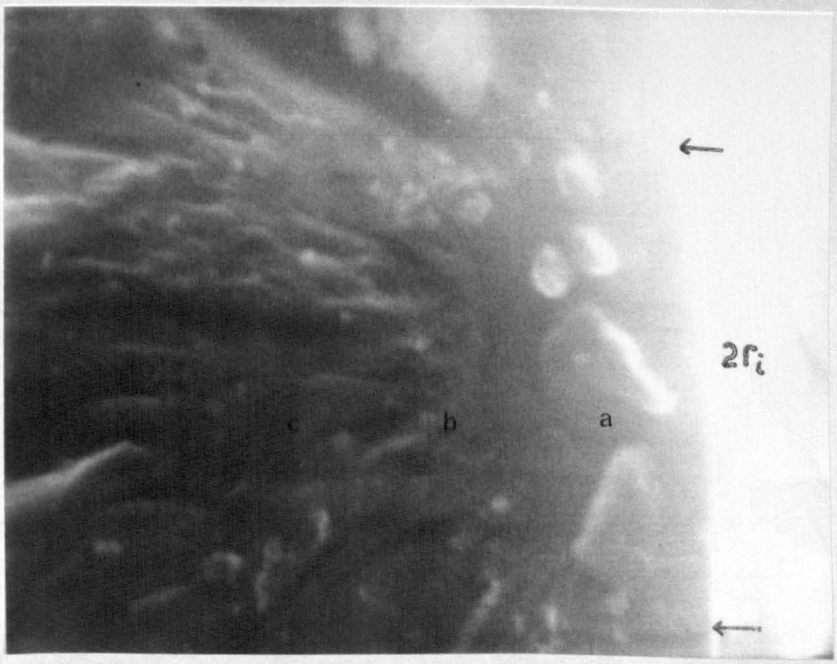

FIGURE 7: SEM fractograph showing origin of fracture in the bulk of the fibre.

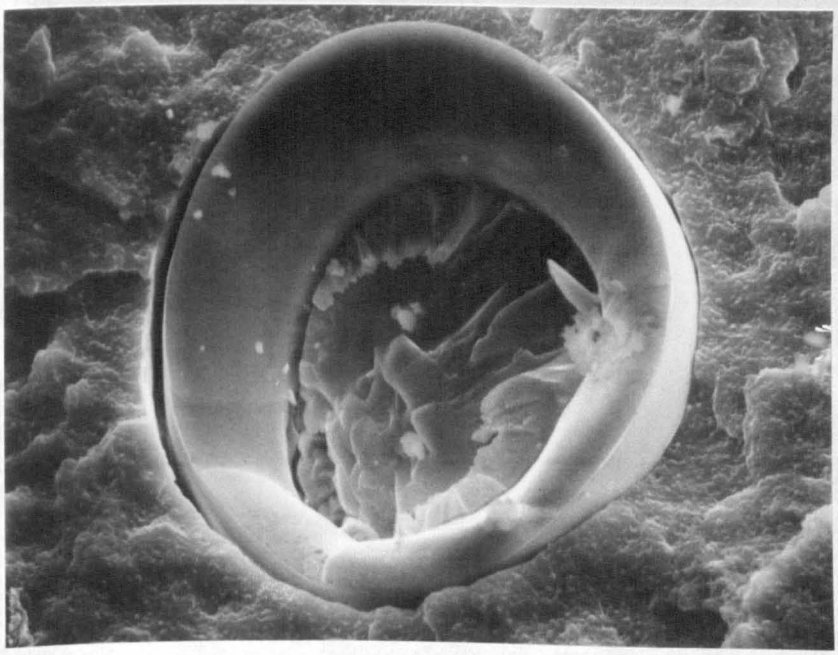

FIGURE 8

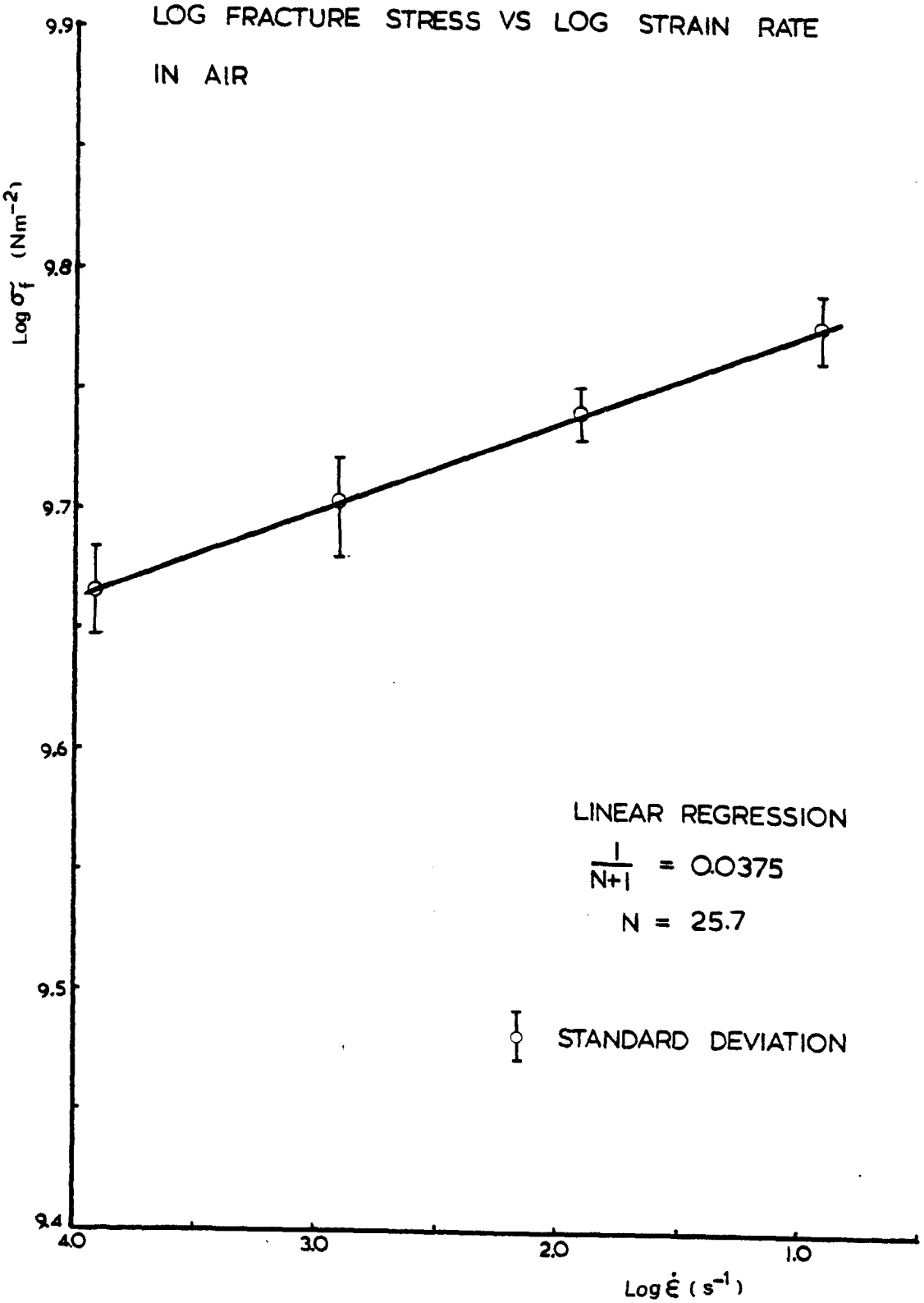
LOG FRACTURE STRESS VS LOG STRAIN RATE
IN AIR
9.9
9.8
9.7
9.6
9.5
9.4
Log σ_f (Nm^{-2})
4.0
3.0
2.0
1.0
Log $\dot{\epsilon}$ (s^{-1})
LINEAR REGRESSION
$\frac{1}{N+1}$ = 0.0375
N = 25.7
STANDARD DEVIATION

FIGURE 9

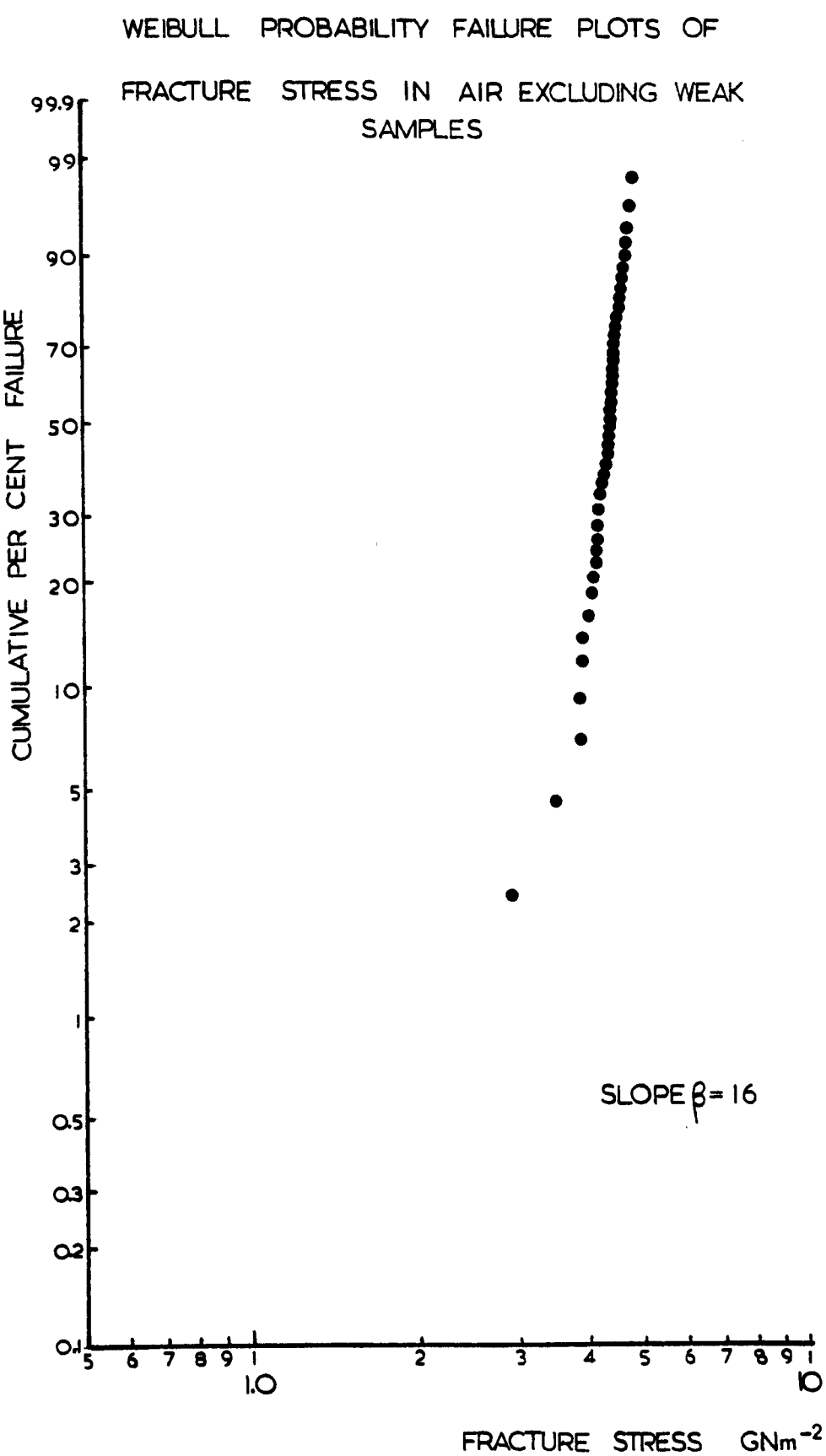
WEIBULL PROBABILITY FAILURE PLOTS OF FRACTURE STRESS IN AIR EXCLUDING WEAK SAMPLES
CUMULATIVE PER CENT FAILURE
99.9
99
90
70
50
30
20
10
5
3
2
1
0.5
0.3
0.2
0.1
SLOPE β = 16
5 6 7 8 9 1 2 3 4 5 6 7 8 9 1
1.0
10
FRACTURE STRESS GNm⁻²

FIGURE 10

DESIGN DIAGRAM IN AIR EXCLUDING LARGE FLAWS FOR 0.5m GAUGE LENGTH

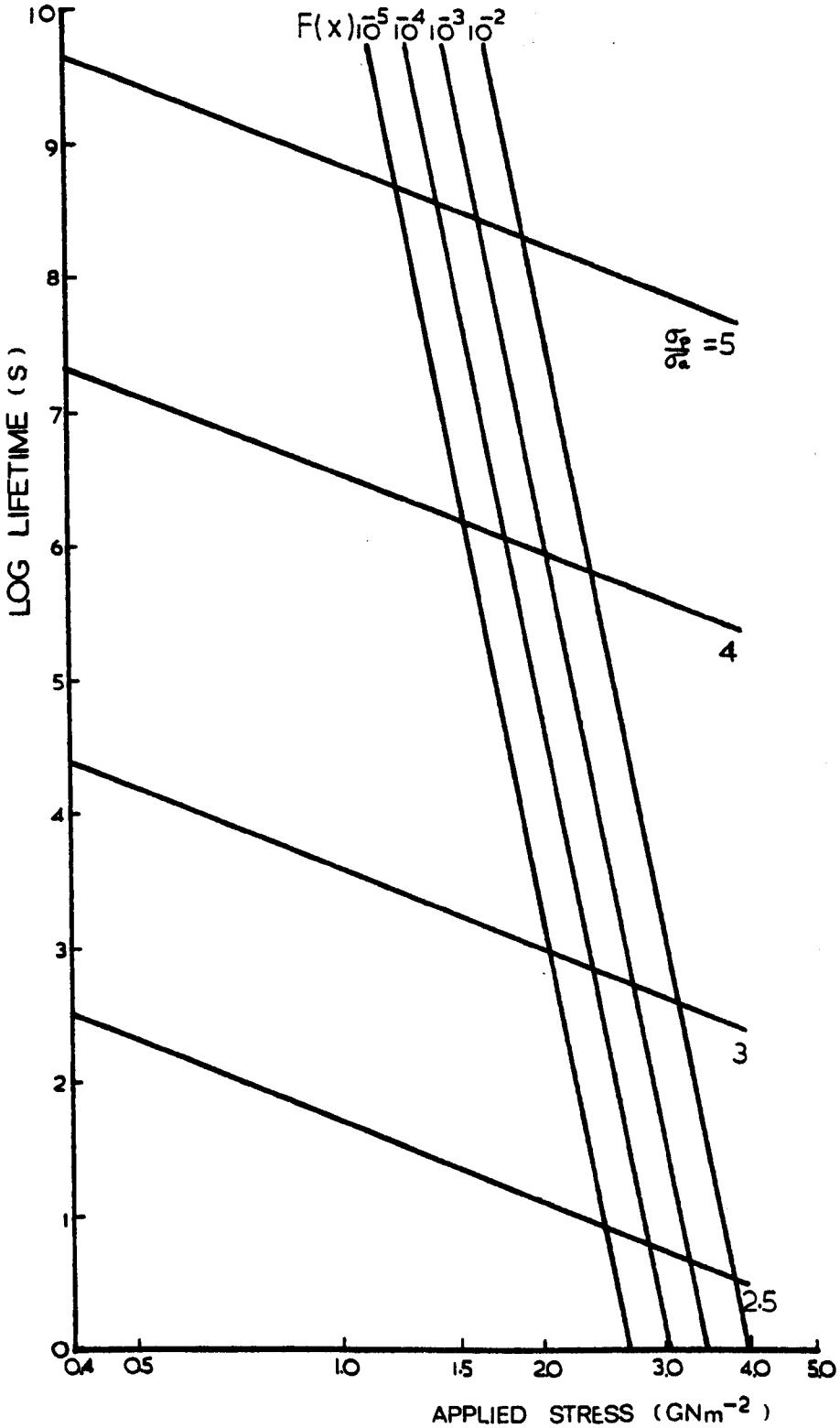

FIGURE 11

WEIBULL PROBABILITY FAILURE PLOTS OF FRACTURE STRESS FOR VARIOUS ANGLE OF TWISTS

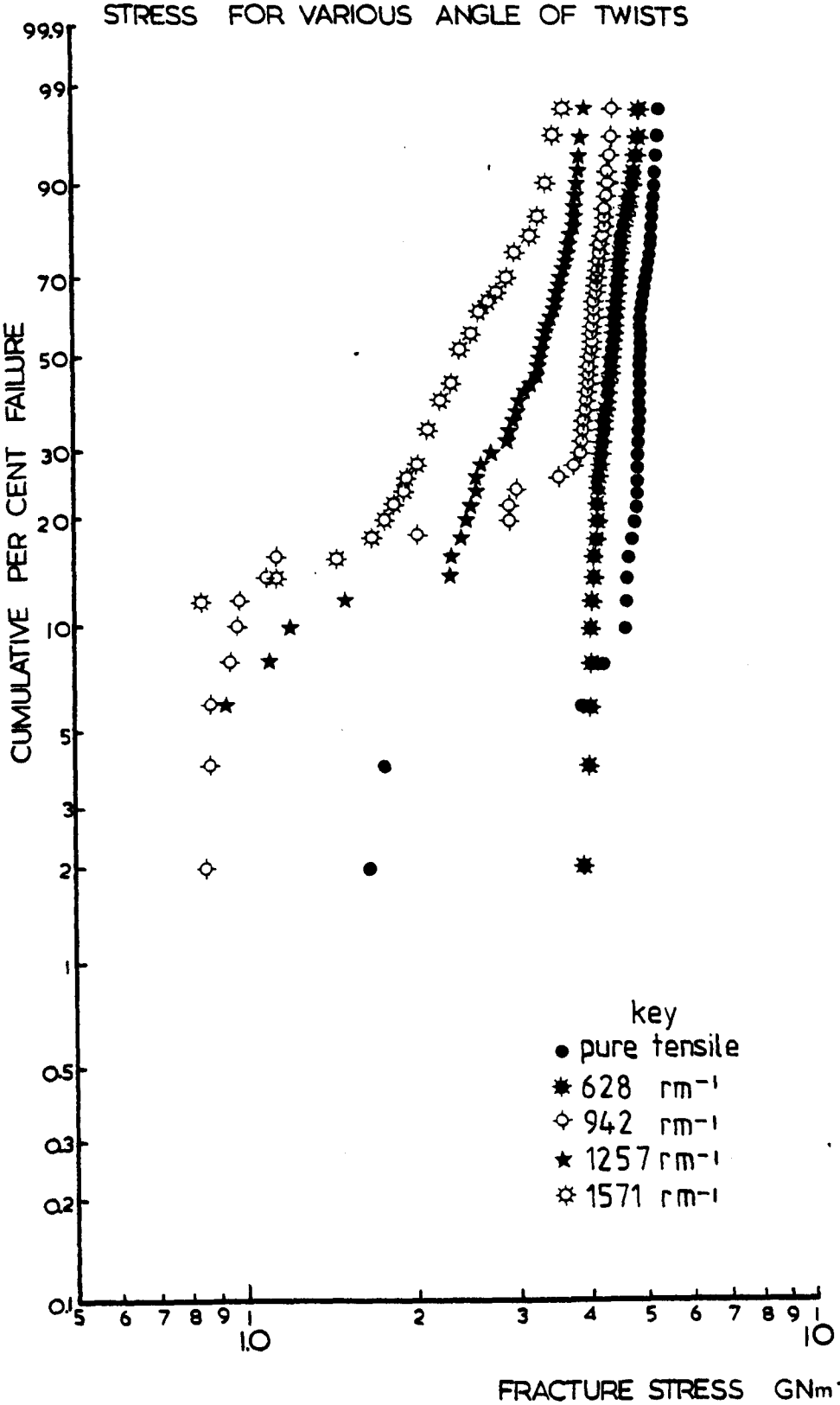

FIGURE 12

WEIBULL PROBABILIY FAILURE PLOTS OF FRACTURE STRAIN FOR VARIOUS ANGLE OF TWISTS

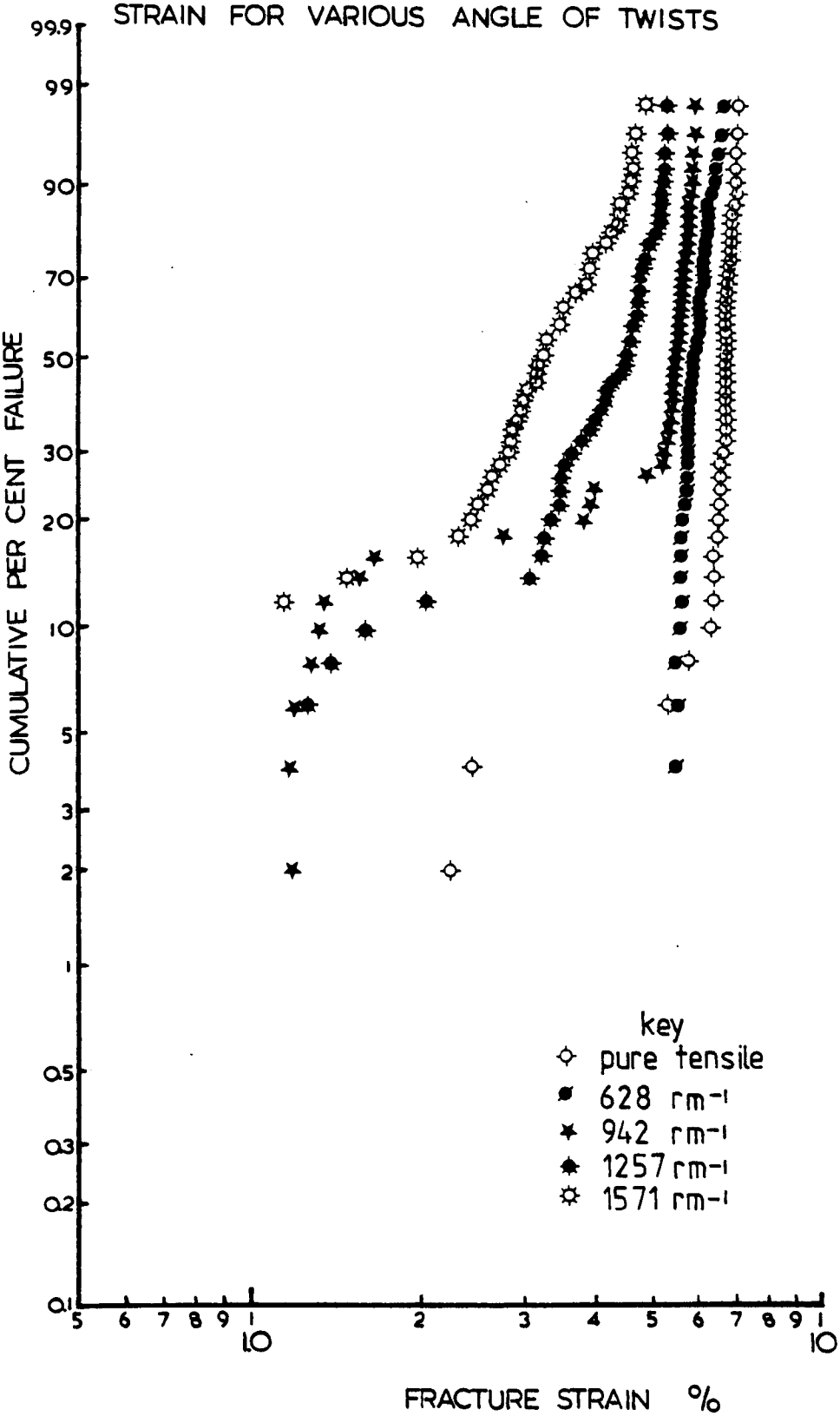

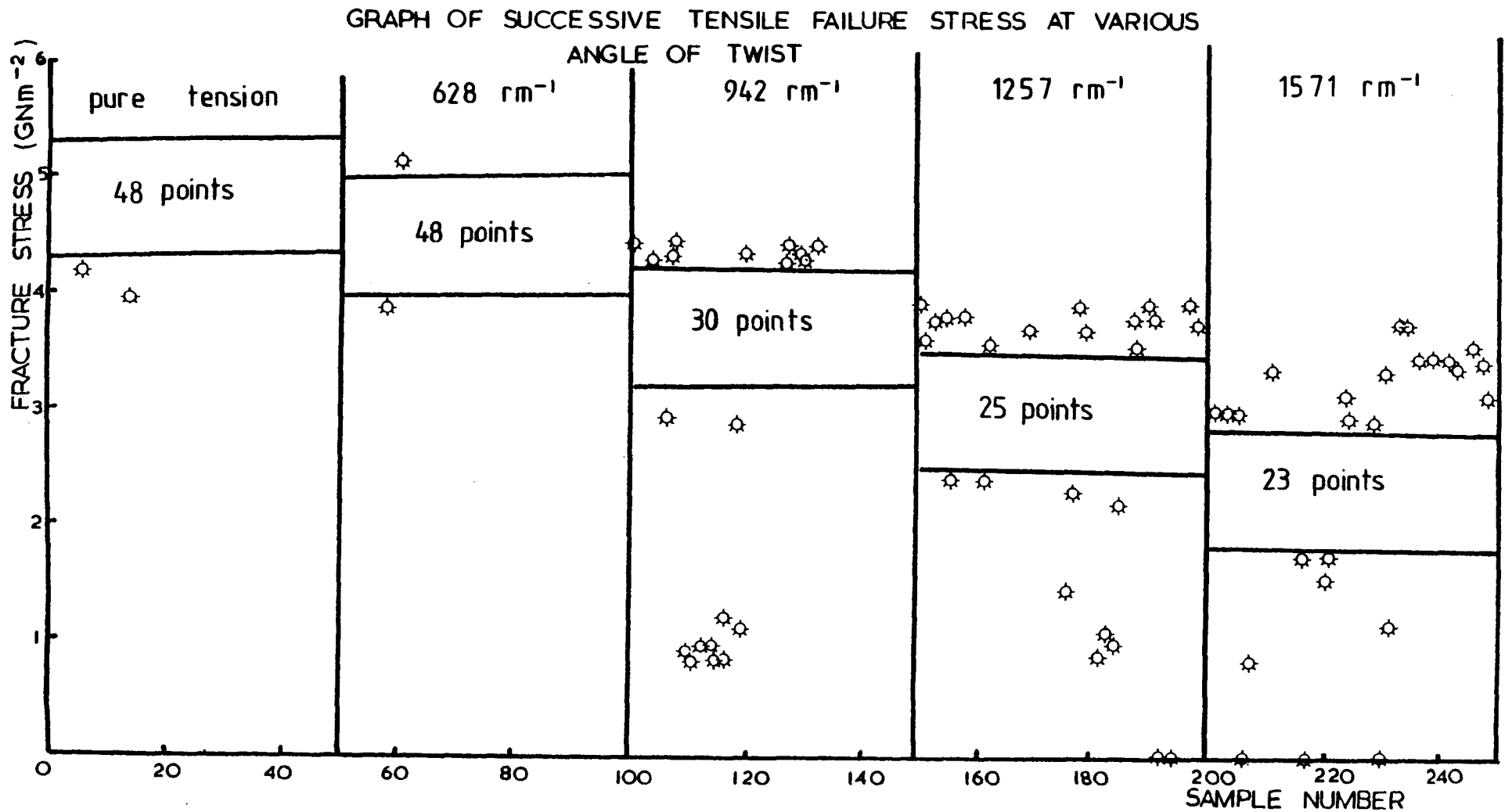
GRAPH OF SUCCESSIVE TENSILE FAILURE STRESS AT VARIOUS ANGLE OF TWIST
FRACTURE STRESS (GNm⁻²)
pure tension
628 rm⁻¹
942 rm⁻¹
1257 rm⁻¹
1571 rm⁻¹
48 points
48 points
30 points
25 points
23 points
0
1
2
3
4
5
6
20
40
60
80
100
120
140
160
180
200
220
240
SAMPLE NUMBER

FIGURE 13

FIGURE 14

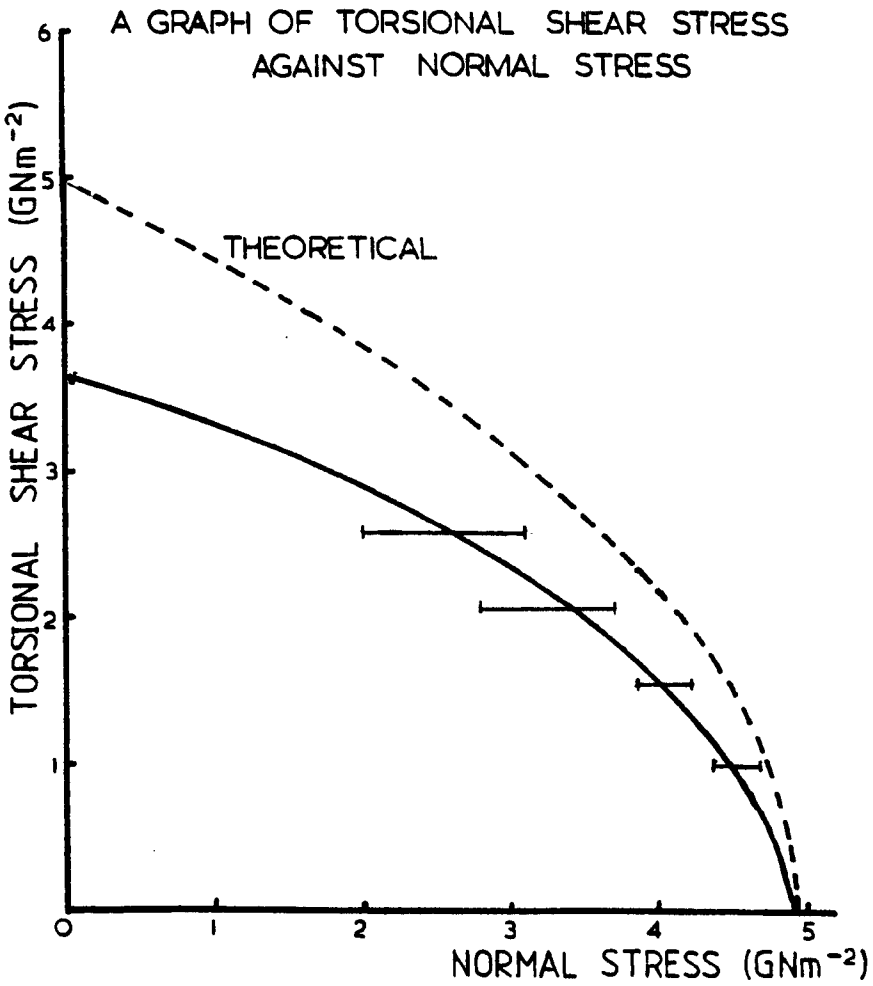
A GRAPH OF TORSIONAL SHEAR STRESS AGAINST NORMAL STRESS
TORSIONAL SHEAR STRESS (GNm⁻²)
NORMAL STRESS (GNm⁻²)
THEORETICAL
0
1
2
3
4
5
6

FIGURE 15

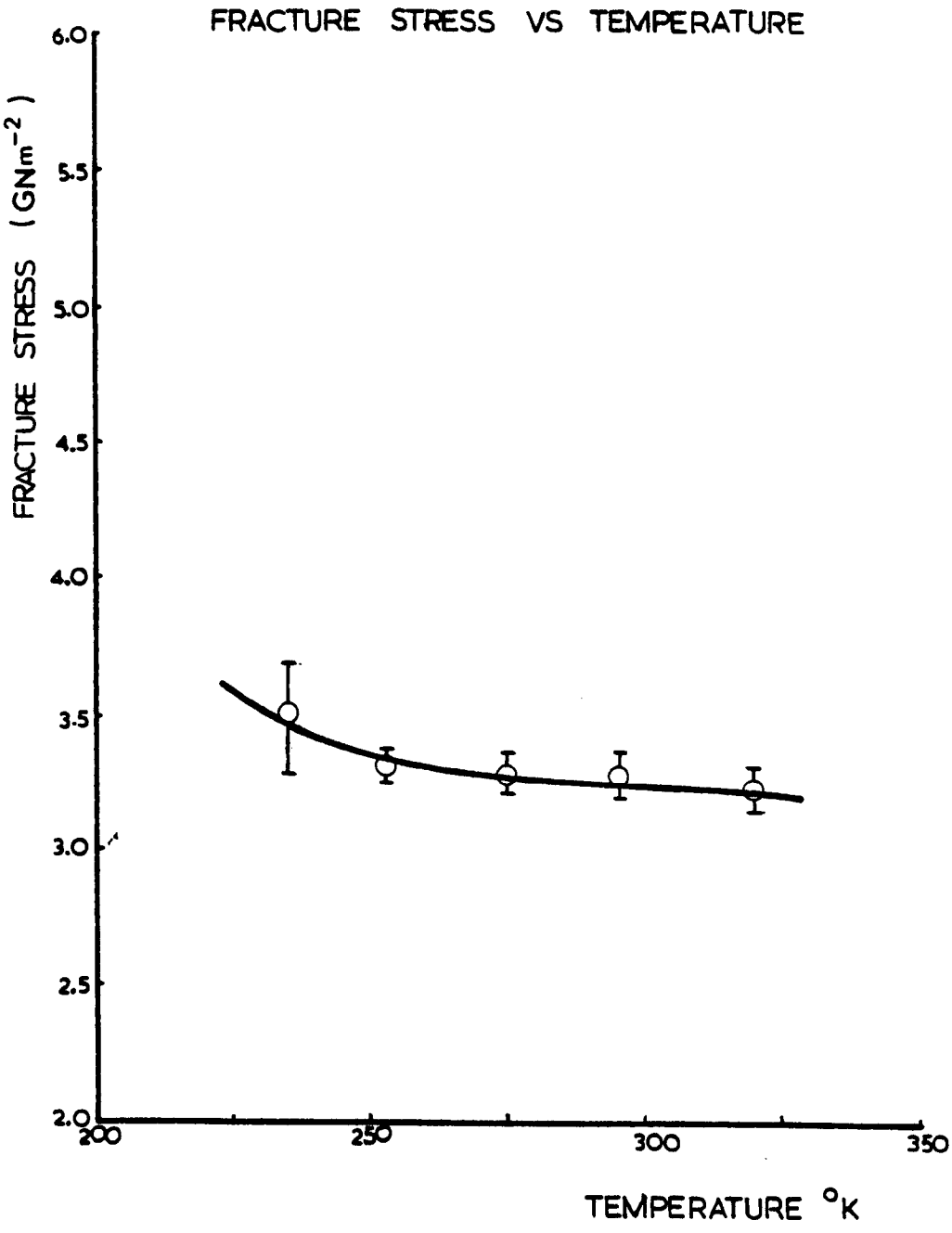
FRACTURE STRESS VS TEMPERATURE
FRACTURE STRESS (GNm^{-2})
6.0
5.5
5.0
4.5
4.0
3.5
3.0
2.5
2.0
200
250
300
350
TEMPERATURE °K

FIGURE 16

WEIBULL PROBABILITY FAILURE PLOTS OF FRACTURE STRESS FOR VARIOUS pH VALUES

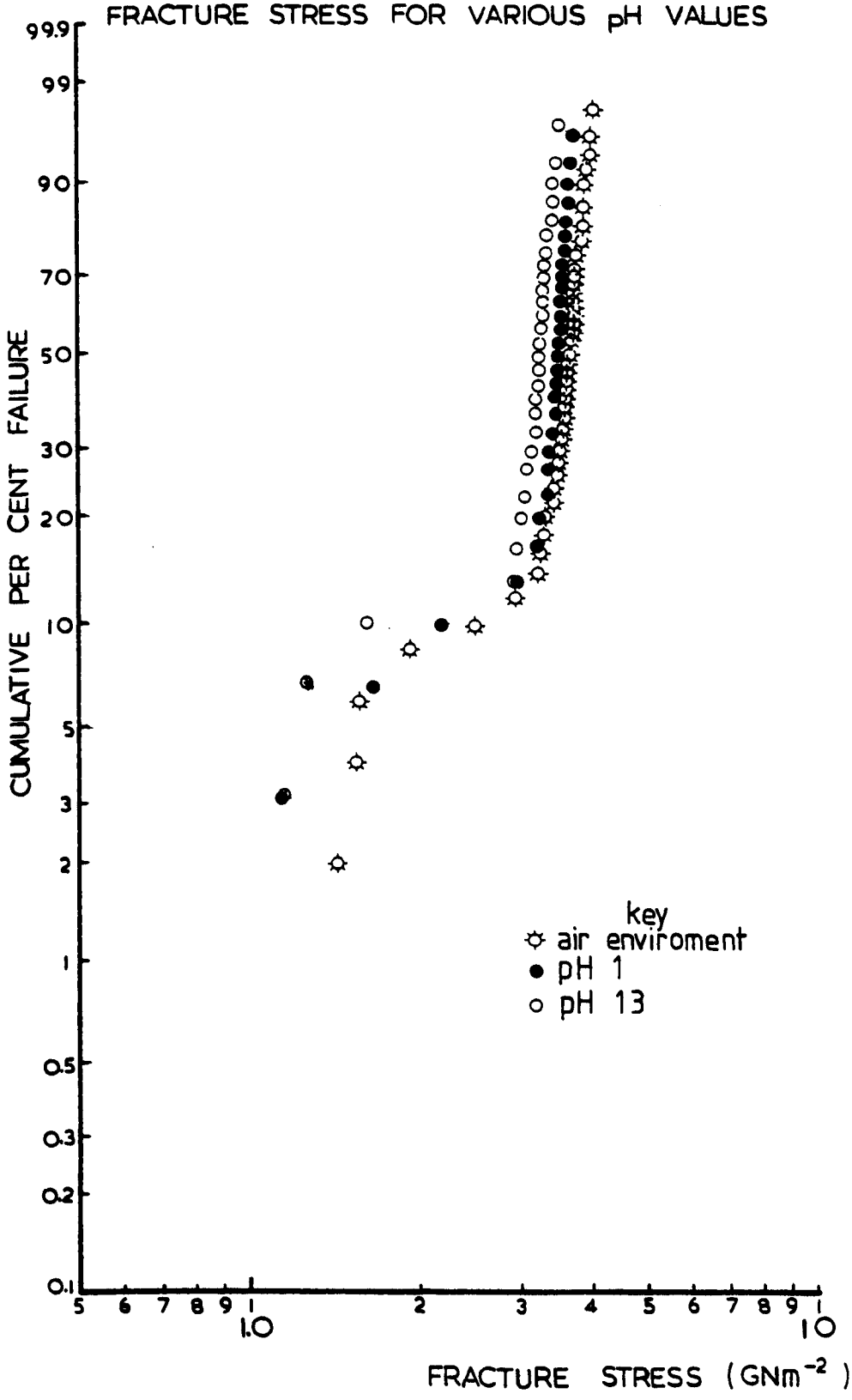

FIGURE 17 (a)

LOG FRACTURE STRESS VS LOG STRAIN RATE

IN 1.0N SODIUM HYDROXIDE SOLUTION

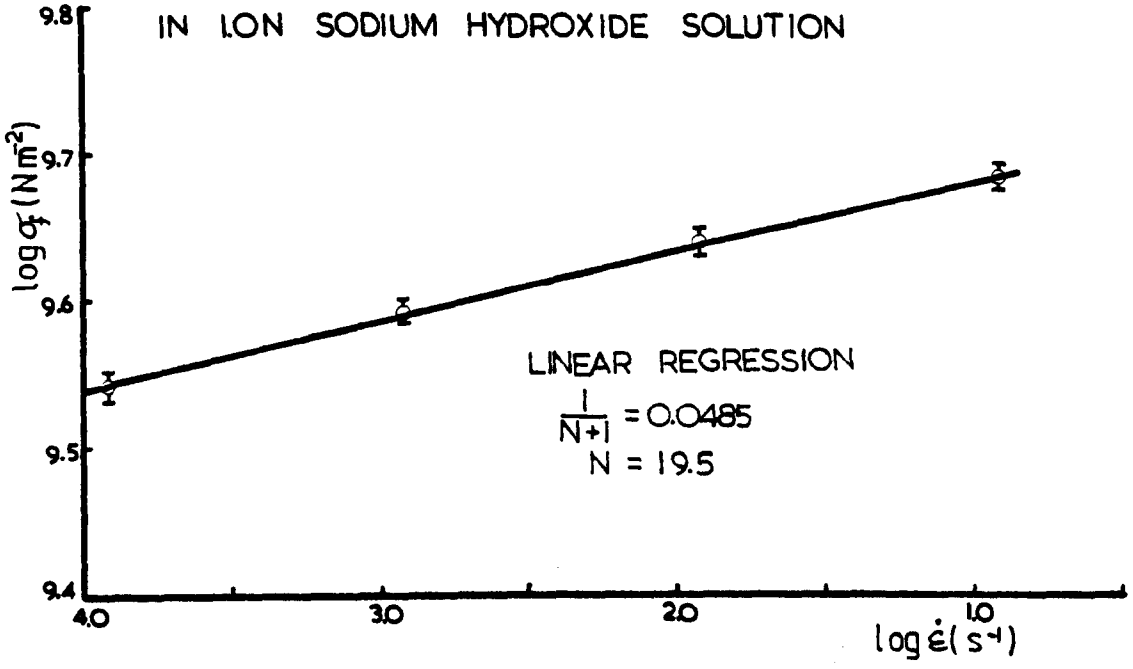

FIGURE 17 (b)

LOG FRACTURE STRESS VS LOG STRAIN RATE

IN 5.0N SODIUM HYDROXIDE SOLUTION

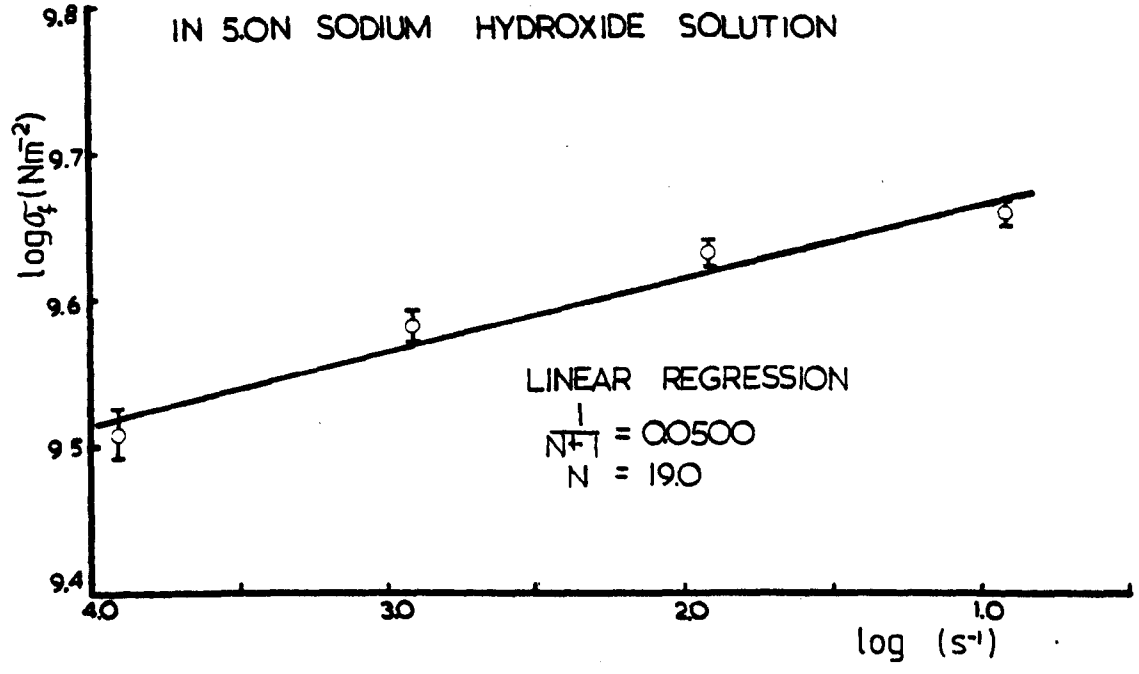

FIGURE 17 (c)

LOG FRACTURE STRESS VS LOG STRAIN RATE

IN DISTILLED WATER

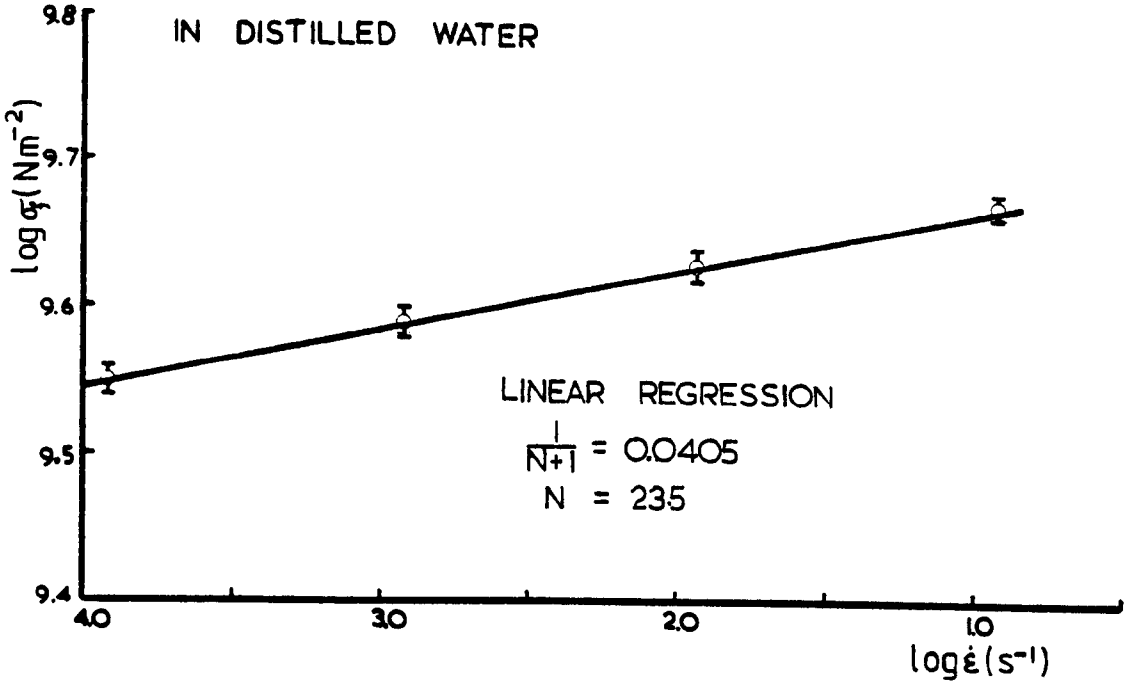

FIGURE 17 (d)

LOG FRACTURE STRESS VS LOG STRAIN RATE

IN O.IN SODIUM HYDROXIDE SOLUTION

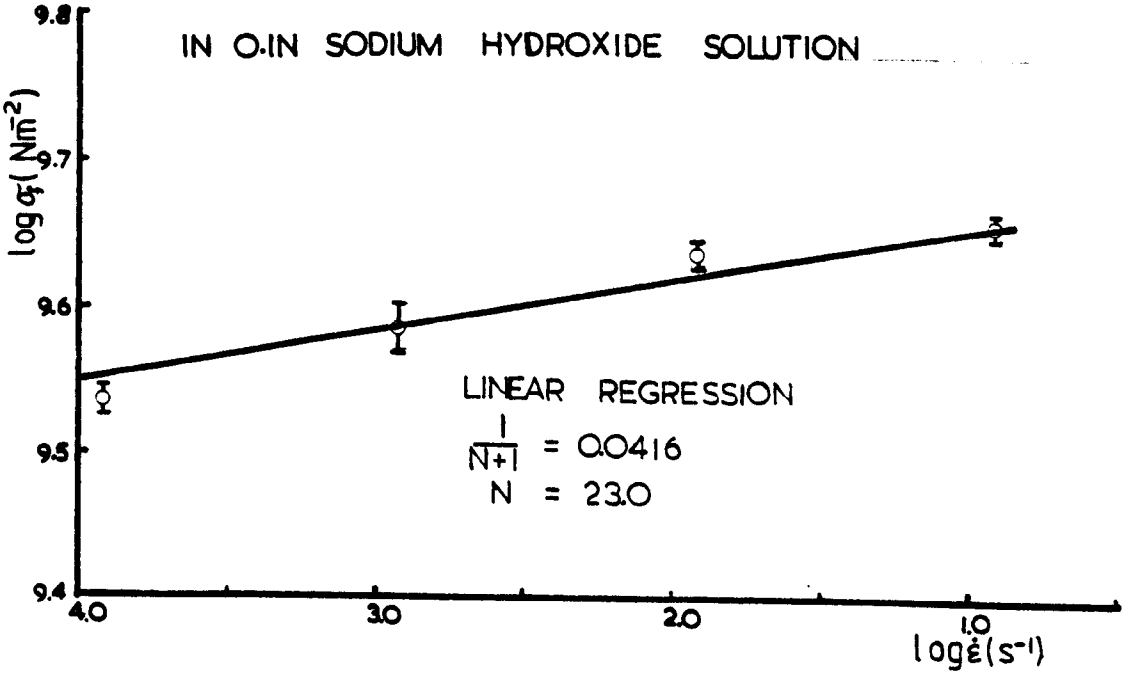

FIGURE 17 (e)

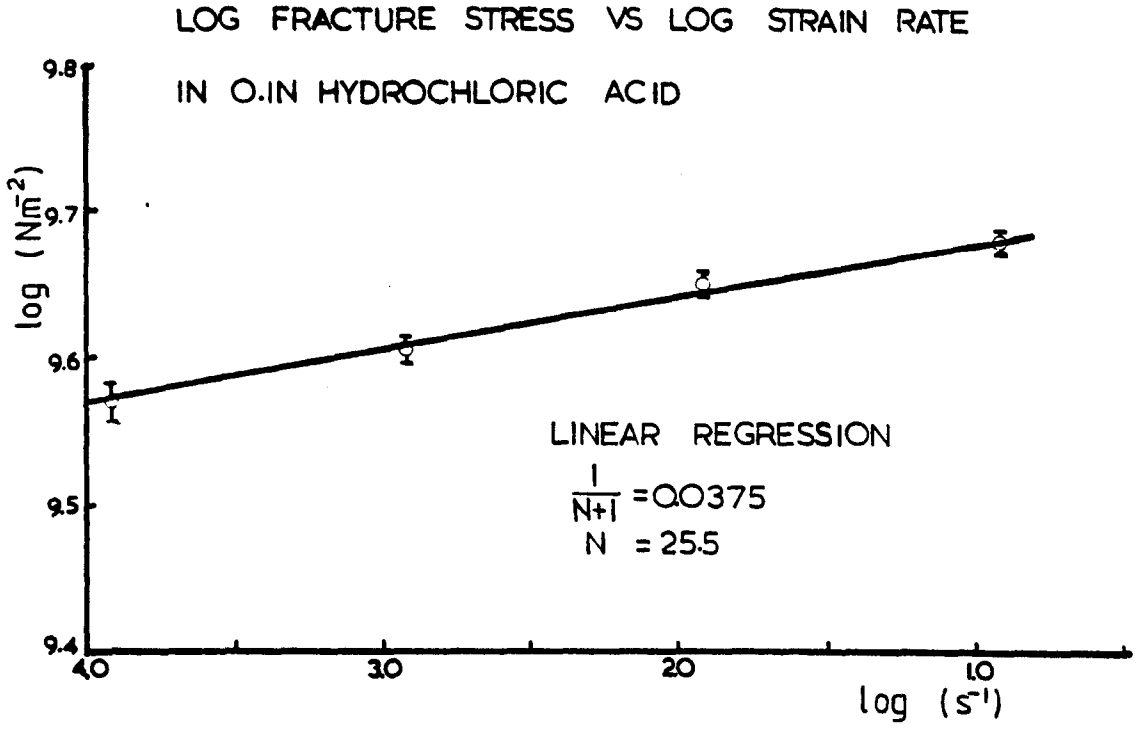

FIGURE 17 (f)

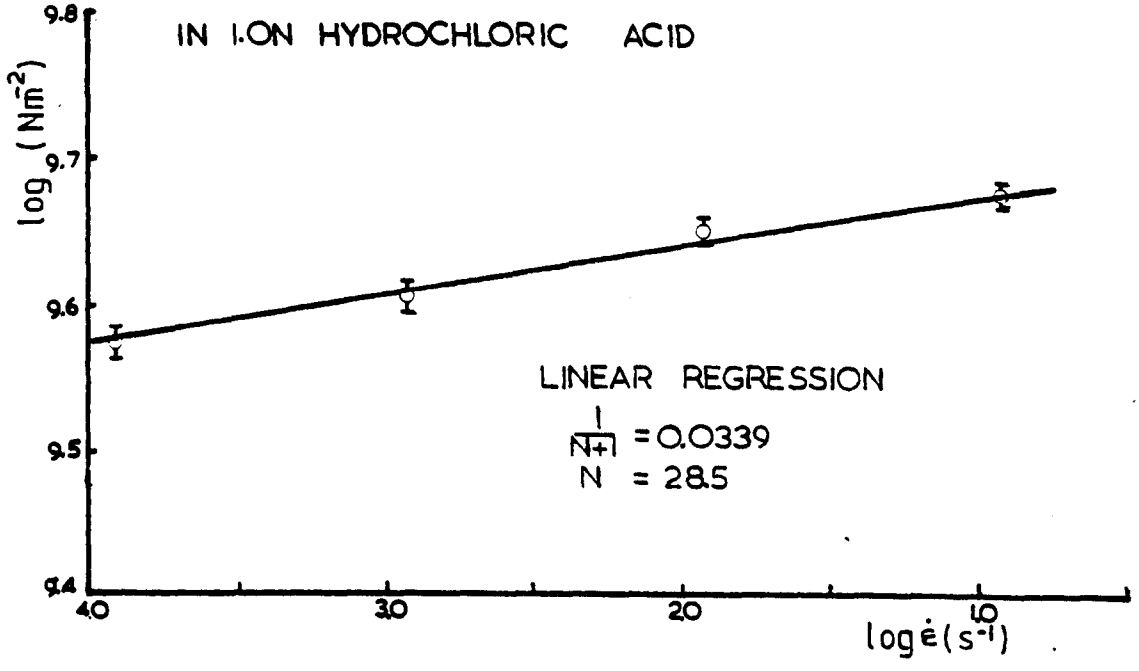

FIGURE 18

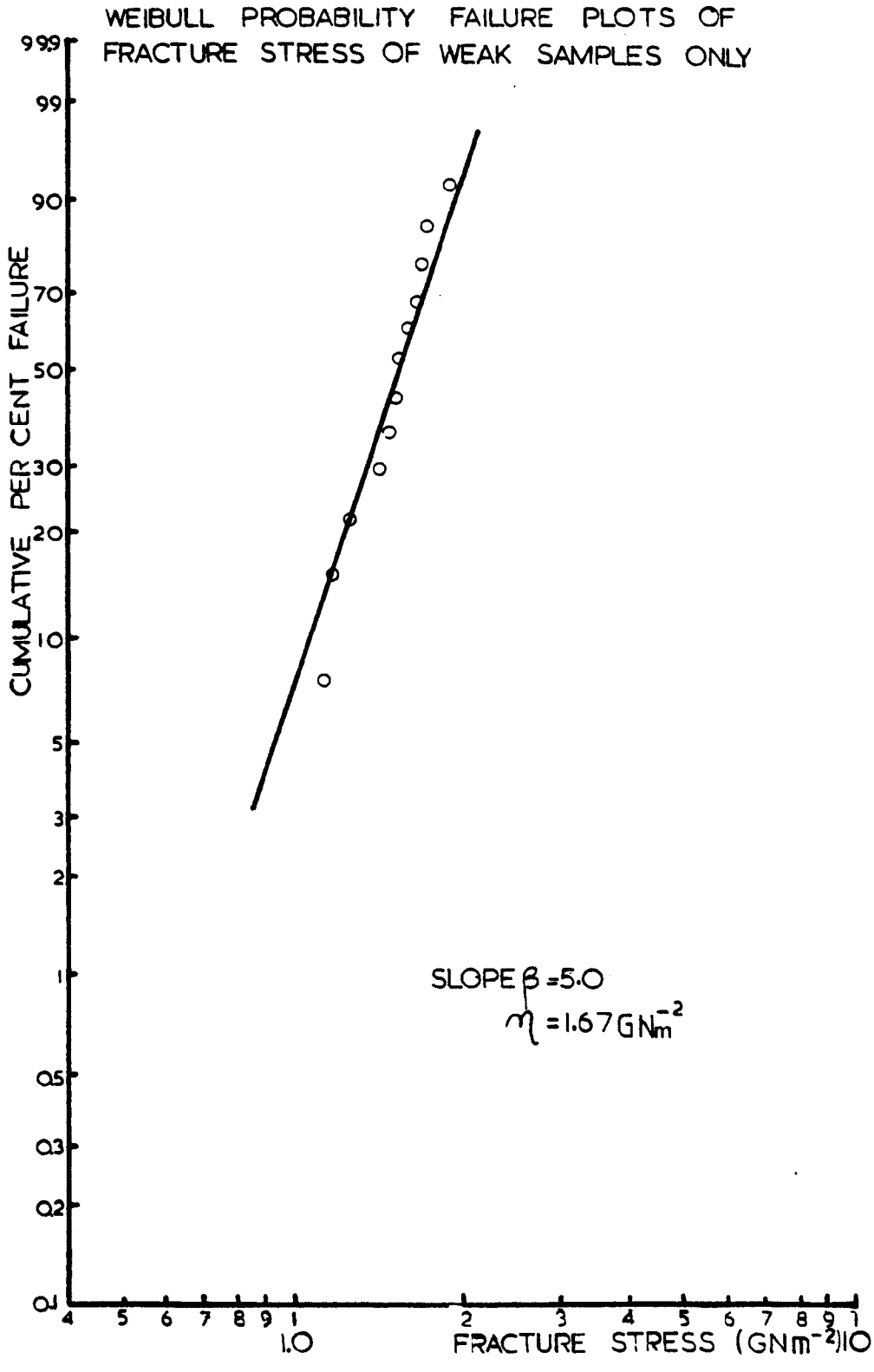
WEIBULL PROBABILITY FAILURE PLOTS OF
FRACTURE STRESS OF WEAK SAMPLES ONLY
CUMULATIVE PER CENT FAILURE
999
99
90
70
50
30
20
10
5
3
2
1
0.5
0.3
0.2
0.1
SLOPE β =5.0
η =1.67 GNm⁻²
4 5 6 7 8 9 1 2 3 4 5 6 7 8 9 1
1.0
FRACTURE STRESS (GNm⁻²) 10

FIGURE 19

GRAPH OF CRITICAL FLAW SIZE VS FRACTURE STRESS

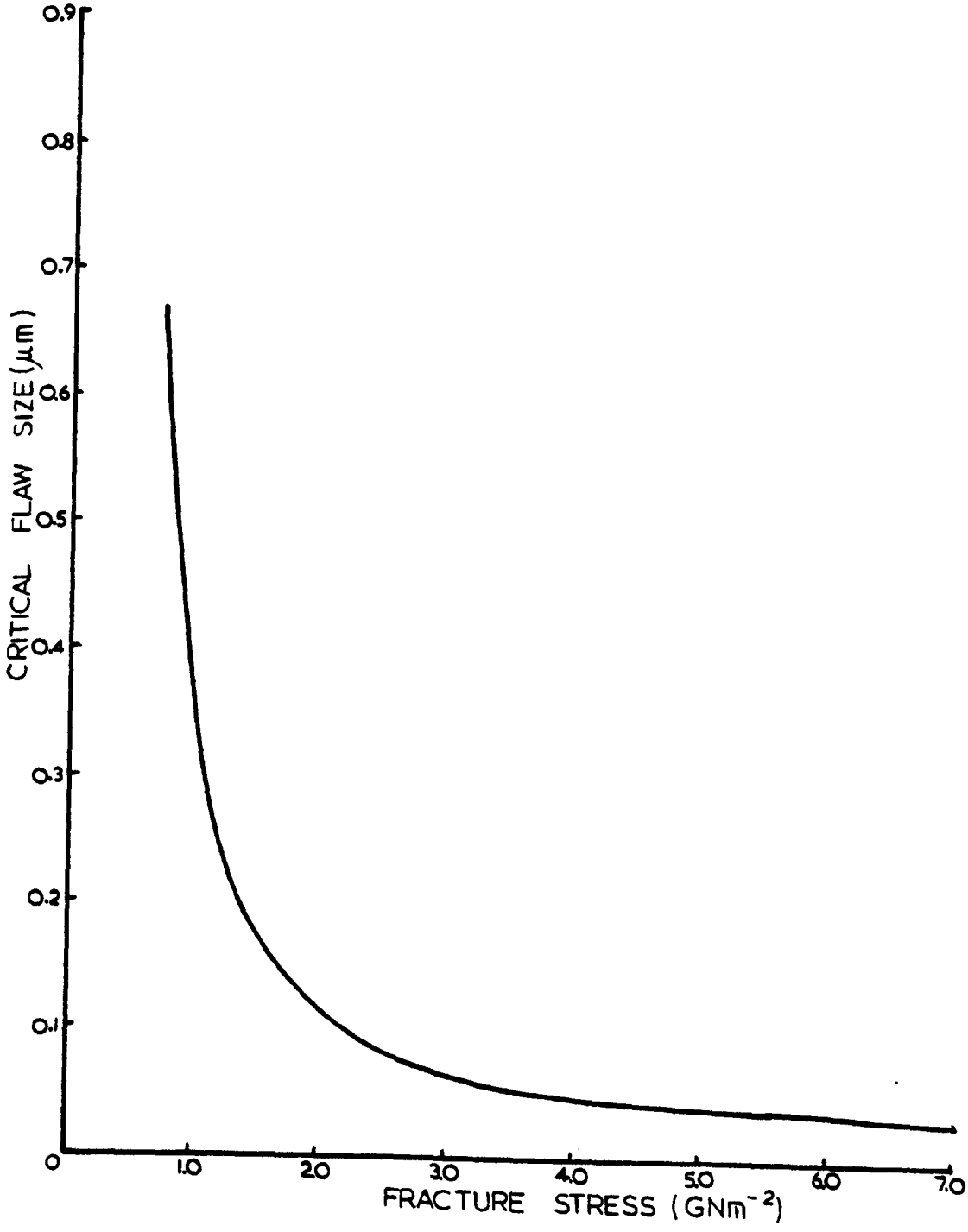

FIGURE 20

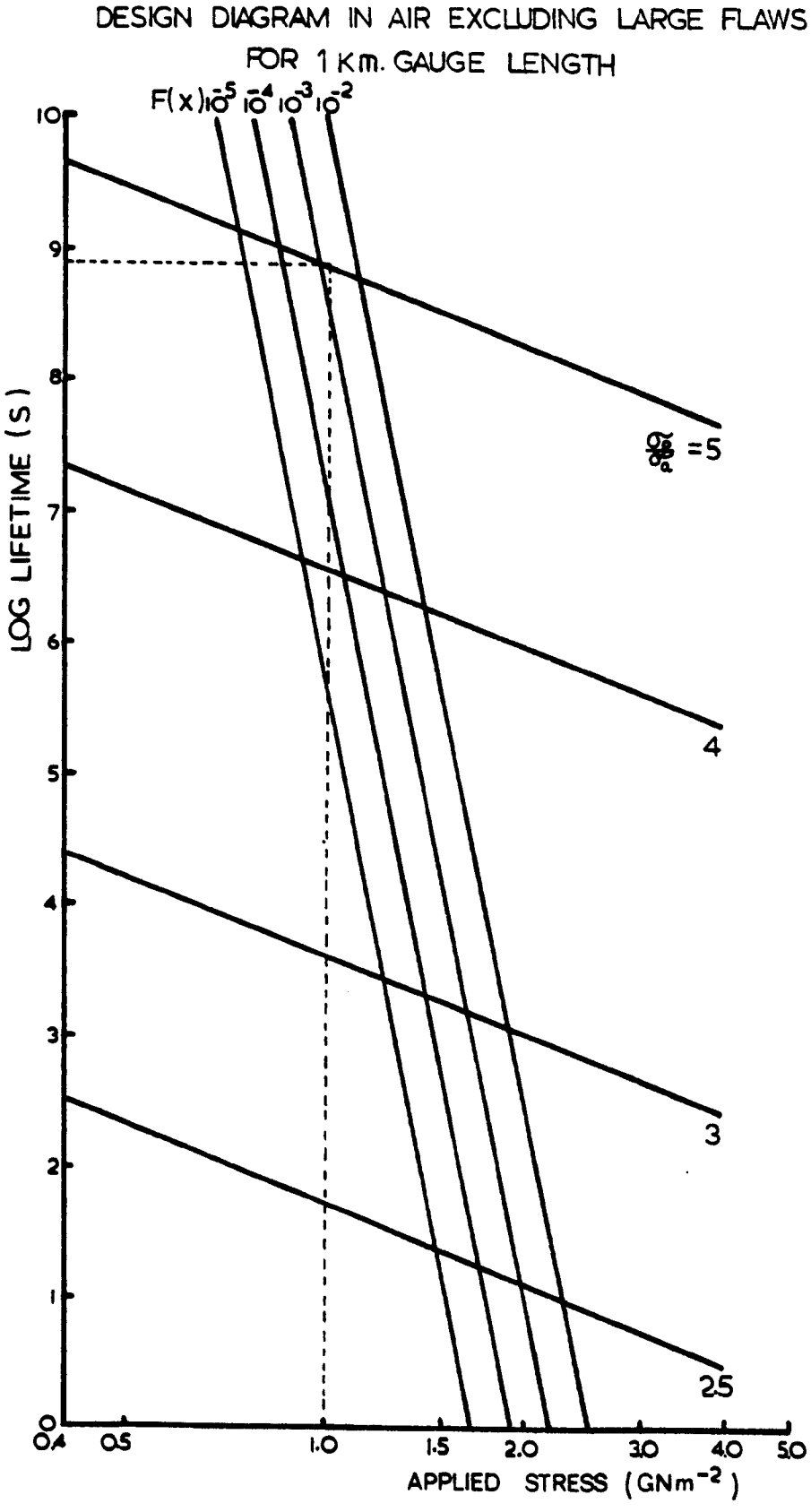
DESIGN DIAGRAM IN AIR EXCLUDING LARGE FLAWS
FOR 1 Km. GAUGE LENGTH
F(x) 10^-5 10^-4 10^-3 10^-2
LOG LIFETIME (S)
10
9
8
7
6
5
4
3
2
1
0
σ/σ_ref = 5
4
3
2.5
0.4
0.5
1.0
1.5
2.0
3.0
4.0
5.0
APPLIED STRESS (GNm^-2)

FIGURE 21

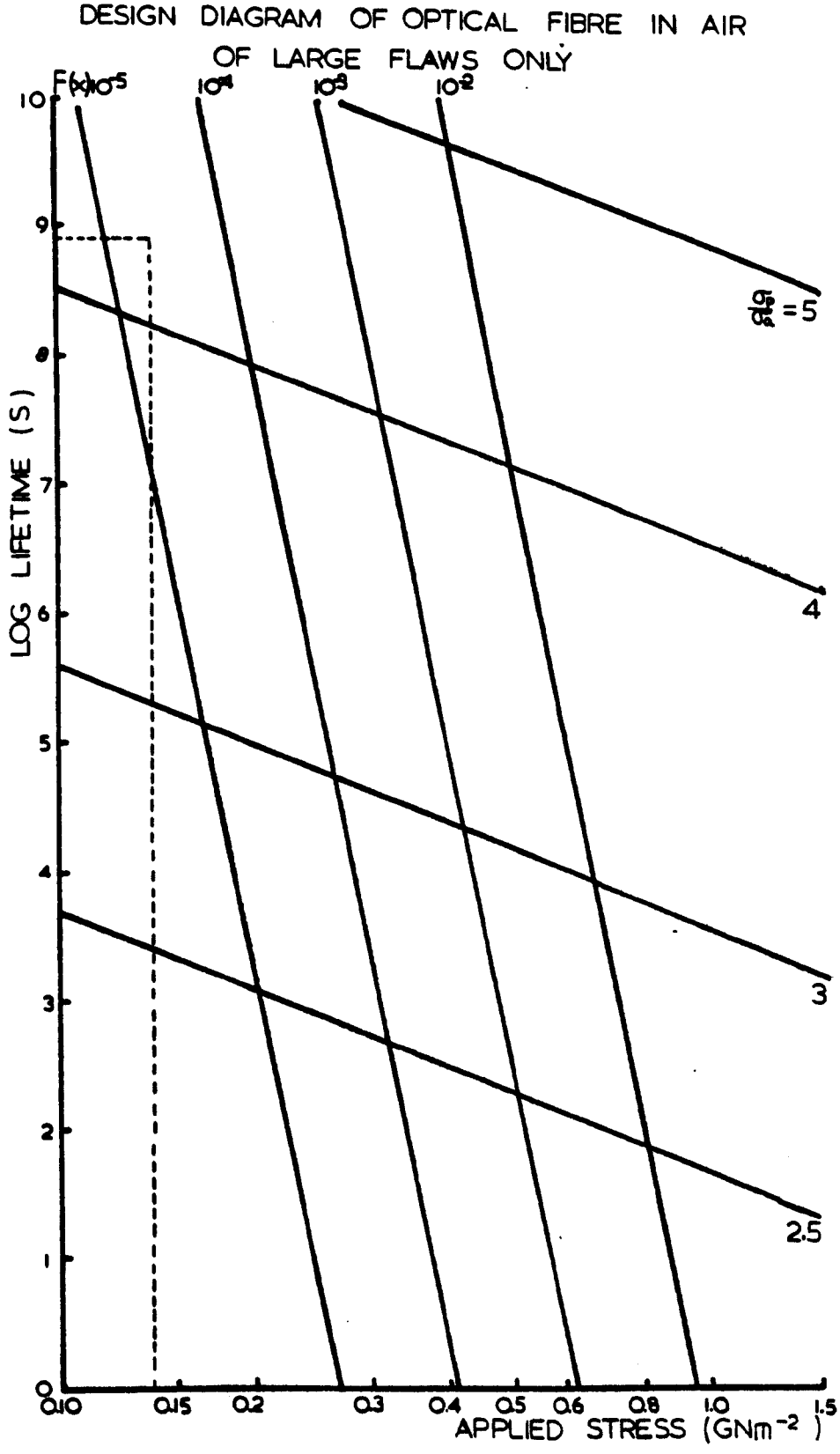
DESIGN DIAGRAM OF OPTICAL FIBRE IN AIR
OF LARGE FLAWS ONLY
F(x)10^-5
10^-4
10^-3
10^-2
LOG LIFETIME (S)
10
9
8
7
6
5
4
3
2
1
0
n=5
4
3
2.5
0.10
0.15
0.2
0.3
0.4
0.5
0.6
0.8
1.0
1.5
APPLIED STRESS (GNm^-2)

FIGURE 22: SEM fractograph of optical fibre failed under combined tension and torsion due to surface flaw.

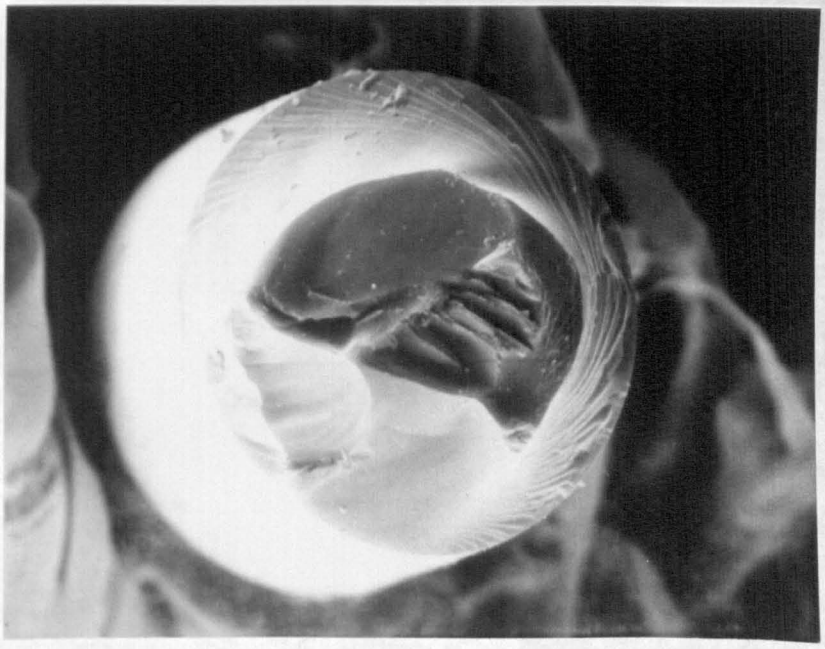

FIGURE 23: Fractograph of optical fibre failed under combined tension and torsion due to internal flaw.

REFERENCES

1. T H Mairman. Nature, 187, 494 (1960)

2. D W Berriman. Bell Syst. Tech. J., 43, 1469 (1964); 44, 2117 (1965).

3. A C S van Heel, A New Method of Transporting Optical Images without Aberrations. Nature 2. Jan. 1954, vol. 173, p.39.

4. H H Hopkins and N S Kapany. A Flexible Fibrescope Using Static Scanning: Nature, 2 January 1954, vol. 173, pp 39-41.

5. K C Kao, G A Hockham: Dielectric-Fibre Surface Waveguides for Optical Frequencies. IEE Proceedings, July 1966. Vol. 113. No.7 pg 1151-1578.

6. R D Maurer. Proc. IEE, 123, 581 (1976)

7. S M Wiederhorn. "Subcritical Crack Growth in Ceramics". pg. 613-46 in Fracture Mechanics of Ceramics. Vol.2. Edited by R C Bradt, D P Hasselmann, F F Lango, Plenum Press, New York, 1974.

8. A A Griffiths. Phil. Trans. A221, 163. (1920)

9. W Weibull. "A Statistical Distribution Function of Wide Applicability". J.Appl.Mech. 18, pg 293-97. (1951)

10. A G Evans and S M Wiederhorn. "Proof Testing of Ceramic Materials - An Analytical Basis for Failure Prediction". Int.J. Fract. 10, pg 379-92. (1974)

11. W J Duncan, P W France and K J Beales. "Effect of Service Environment on Proof Testing of Optical Fibres". To be published.

12. R D Maurer. "Effect of Dust on Glass Fibre Strength" App. Phy. Letters. Vol. 30, No.2, Jan. 1977.

13. J J Mecholsky, S W Freiman, and R W Rice
Journ. Am, Ceram. Soc. 57, 1974, pg 440.

14. S M Wiederhorn, H Johnson, A M D
"Fracture of Glass in Vacuum". J. Am. Ceram. Soc.
57(8) pg 336-41 (1974).

15. J J Mecholsky Jun., S W Freiman, R W Rice.
"Fracture Surface Analysis of Ceramics".
Journ. of Mat. Sc. 11 (1976) pg 1310-1319.

16. H Schonhorn, C R Kurkjian, R E Jaeger,
R V Albarino and F V DiMarcello. App. Phys. Letter,
29, 712, (1976).

17. R Kashyap, M H Reeve, S Hornung, J Russell and
J Titchmarch. I. O.O.C. 1981.

18. B A Proctor, J. Whitney and J W Johnson.
"The Strength of Fused Silica". Proc. R. Soc.
London. Ser. A. 297 (1451) pg 534-57 (1967).

19. S M Widernorn, H Johnson. Effect of Electrolyte
pH on Crack Propagation in Glass. J. of Am. Ceram.
Soc. Vol. 56, No. 4, 1973.